

The establishment of assay system of renal senescence
and its regulation

腎臓の老化の評価システムの確立とその調節

東京大学 大学院 博士課程

医学系研究科内科学専攻（腎臓内科学）

平成 18 年 4 月入学

No. 41-67384

池田洋一郎

Table of Contents

ABSTRACT	2
INTRODUCTION	3
GENERAL CHANGES IN SENESENCE	3
NO DEFINITE REPORTS OF LONG LIFE-SPAN CAUSED BY HIGH LEVEL OF ANTIOXIDANT	4
CARBONYL STRESS, PRECURSOR OF AGES : BYSTANDER OR CULPRIT?	5
AGE-RELATED RENAL PHENOTYPE	6
NEED FOR ESTABLISHMENT OF ASSAY SYSTEM OF CELLULAR SENESENCE	8
MATERIALS AND METHODS	8
RESULTS	18
VALIDATION OF CELLULAR SENESENCE IN PRIMARY CULTURED TUBULAR CELLS	18
BENEFICIAL EFFECT OF GLO1 TO SENESENCE OF TUBULAR CELLS	20
THE AGE-RELATED MORPHOLOGICAL CHANGE IN INTERSTITIUM OF HUMAN KIDNEY	21
VALIDATION OF SENESENT STATUS IN AGED KIDNEY	21
AMELIORATION OF SENESENT PHENOTYPE IN AGED-KIDNEY OF GLO1 TRANSGENIC RATS	22
OVEREXPRESSION OF GLO1 AMELIORATES OXIDATIVE STRESS IN AGED KIDNEY	24
DISCUSSION	25
DISCLOSURE	30
ACKNOWLEDGMENTS	30
REFERENCES	31
FIGURE LEGENDS AND FIGURES	35

Abstract

While renal functions deteriorate with age, little is known about manifestations and mechanisms of renal senescence. Advanced glycation end-products (AGEs) are well known to play a pivotal role in senescence. I hypothesized that primary reduction of AGEs lead to less phenotype of senescence, and investigated a role of glyoxalase I (GLO1), which detoxifies chiefly precursor of AGE, dicarbonyl compounds, in the aging process of the kidney. First, I established the system to assess renal senescence, which included halt of the cellular proliferation (*in vitro*), interstitial thickening (*in vivo*), elevated transcript and protein expression levels of p53, p21^{WAF1/CIP1} and p16^{INK4A}, and elevated positive rate of senescence-associated β -galactosidase (SABG) staining. Next, the renal phenotype of histological senescence was assessed by reviewing the human renal biopsy specimen from the patients of whom renal function was less impaired. Interstitial thickening was demonstrated to be the renal histological manifestation of senescence. Finally, primary regulation of AGEs by overexpression or knockdown of GLO1 was demonstrated to affect cellular or histological status of renal senescence. In conclusion, I clarified the renal senescence by senescent marker expression and cellular and pathological phenotypes *in vivo* and *in vitro*, and demonstrated amelioration of renal senescence by GLO1 overexpression through reduction of AGE accumulation.

Introduction

General changes in senescence

It has long been a wonderful dream to prevent or retard aging, and to achieve longevity. Primary somatic cells grown *in vitro* do not proliferate indefinitely. Instead, after a period of rapid proliferation, cell division rate slows, and ultimately ceases altogether, with the cells becoming unresponsive to mitogenic stimuli, the condition of which is called “Hayflick’s phenomenon.” This process, cellular senescence, is usually associated with a well-defined accompanying phenotype - increased cell size, distinctive flattened morphology, and is also associated with wide changes in gene expression including upregulation of cell cycle regulators such as p53, p21^{WAF1/CIP1} or p16^{INK4A}, and positivity in senescence-associated β -galactosidase (SABG) staining (1, 2). The mechanisms of senescence have been investigated so far in studies both *in vitro* and *in vivo*. It is speculated that replicative senescence of cells and histological aging may share common molecular mechanisms. It is generally believed that cellular senescence reflects some of the changes that occur during the aging of organisms, and senescent cells are detected *in vivo* at the sites where age-related pathological change is found, such as atherosclerotic lesions (3) and benign prostate hyperplasia (4). In tissues from senescent organisms, Hayflick’s phenomenon cannot be observed anymore since it cannot be determined to what extent certain number of specified cells proliferate. Instead, together with the change of cell cycle regulators or positivity in SABG staining, modification of protein such as oxidation, glycation and cross-linking can be observed, whereas age-related morphological changes of tissues are not uniform, depending on organs or organisms.

Few definite reports of long life-span caused by high level of antioxidant

In the mid-1950s, a 'free-radical theory' of aging proposed that endogenous reactive oxygen species (ROS) generated in cells result in cumulative damages (5). It is true that the definitely established method to make animals live long is calorie restriction, which is accompanied by low production of ROS(6). However, the elimination of oxidative stress has not yet succeeded in establishing the definite induction of longevity (7, 8).

There are few definite reports that the overexpression of ROS-eliminating enzymes, such as catalase or superoxide dismutases such as Cu/Zn-SOD (SOD1), Mn-SOD (SOD2), or continuous administration of antioxidants such as vitamin C or vitamin E can induce longevity or less phenotype of aging. In one report, maximum life-span of transgenic mice was extended about 20% by overexpression of human catalase targeted to mitochondria (9). But this study was retested and failed to demonstrate the life-extending effect (8). Overexpression of SOD1 and SOD2 also failed to extend the life-span in mice (8). Reviewing the studies of the knockout or transgenic animals of antioxidant enzymes, they concluded only SOD1 knockout mice shortened the life-span and no transgenic mice which overexpressed one antioxidative enzyme or the combination of them didn't realize the life-extending phenomenon (7).

Recent studies revisited this issue. A study utilizing mice deficient in angiotensin type 1 receptor (10) showed longevity of the mice, which was associated with a decrease in oxidative stress of the kidney. Furthermore, the animals with higher levels of ROS live short lives with acceleration of senescence (11). Taken together with these data, ROS may be not totally harmful, or rather, is necessary to cells

for cellular proliferation or host defense (12), suggesting that perturbation of ROS is not an ideal approach to retard the aging process. This notion led to the enthusiasm to seek the much more important target regulating senescence and longevity than ROS. So I gave attention to the by-products generated from universal resource surrounding cells or organelles such as glucose, which is augmented by the production of ROS via glycooxidation. They are advanced glycation end-products (AGEs) and their precursors.

Carbonyl stress, precursor of AGEs : bystander or culprit?

The most widely studied oxidative stress-induced modification to proteins is the formation of carbonyl derivatives(13). Carbonyl formation can occur through a variety of mechanisms including direct oxidation of certain amino-acid side chains and oxidation-induced peptide cleavage. For example, lysine and arginine are well-known amino-acid residues to be easily modified by carbonyl stress as to form N^ε-(carboxyethyl)lysine (CEL) or N^ε-(carboxymethyl)lysine (CML) etc. These modifications can be detected by specific antibodies as previously reported (14, 15). And highly reactive by-products including methylglyoxal (MG), which are generated in the energy metabolism pathway such as glycolysis, contribute synergistically to the formation of AGEs (12). The levels of serum AGEs increase with age in a large cohort of normal subjects, and correlate well with the levels of established markers of oxidative stress and inflammation (16). AGE accumulation is associated with pathologic lesions in age-related diseases, such as diabetes mellitus, Alzheimer's disease, and atherosclerosis (17, 18), and AGEs are likely to be, at least in part, the cause of the aging process rather than the consequence (19). To support this notion, a senescent phenotype was observed in the diabetic kidney

and cultured proximal tubular cells incubated under high-glucose media (20).

Assuming that highly reactive dicarbonyl compounds to form AGEs, accelerate senescence, I hypothesized that the enhancement of their decomposition retards aging. MG, which is highly reactive compound, was decomposed by glyoxalase (GLO) system, which is composed of two enzymes, namely GLO1 and GLO2. They are well conserved in wide variety of species, from yeast to human. The function of the former is to catalyze the conversion of MG together with reduced glutathione (GSH) into S-D-lactoylglutathione, and that of the latter is to catalyze the hydrolysis of S-D-lactoylglutathione to GSH and D-lactic acid (21). GLO1 is reported to be the rate-limiting enzyme of MG catabolism (21). Human GLO1 is dimer with two identical subunits, and each subunit contains 184 amino acid residues with molecular weight of 21kDa (22, 23). The crystal structure of human GLO1 was clarified in 1997 (24) (Fig. 1C, 1D). GLO1 was reported to be expressed ubiquitously in most tissues (25, 26) and to have renoprotective effect under the condition of rat ischemia and reperfusion injury by inhibiting the formation of intracellular MG adducts and oxidative stress (27) , though the detailed distribution analysis of GLO1 in kidney was still to be determined. To support my hypothesis that upregulation of GLO1 can prevent senescence, a recent report showed that overexpression of GLO1 homologue CeGly induce the longevity of C.elegans (11).

Age-related renal phenotype

Declines in renal function, measured by creatinine clearance, occur in "healthy" elderly with the mean decrease in creatinine clearance of 0.75 ml/min/year over time(28). Age-related renal dysfunction is associated with progression of renal fibrosis, and while previous studies elucidated the morphological

changes in the glomerulus in detail, recent studies devoted attention to tubulointerstitial alterations in the aging kidney (29-31). A biological significance of the alterations in the tubulointerstitial compartment in aging is emphasized by the fact that functional impairment of the kidney correlates better with the degree of tubulointerstitial damage than with that of glomerular injury, although these interstitial alterations were demonstrated in rodents and are not the common features of age-related phenotype of human elderly.

There have been few reports of age-related pathology of human elderly. The thickening of Bowman's capsule, proteinaceous casts in distal tubules, cortical interstitial infiltration of macrophages and lymphocytes, and thickening of proximal tubular basement membrane were reported to be features of age-related pathology of rat (32, 33). But these were only descriptive, not quantified, and it was unclear from when these features appeared in the human lives.

Studies of human kidney have shown that the number of functioning nephrons decreases with age, with increasing glomerular size and increasing rate of the development of glomerulosclerosis (34, 35). But these changes were thought to be affected by the genetic background (36, 37) and also were to be determined whether they are actually age-related or subsequent phenotype of underlying disease such as hypertension and hyperglycemia.

What is more, glomeruli are important but minor component of the kidney from the viewpoint of number of cells, and SABG staining or immunohistochemistry of cell cycle regulators such as p53, p21^{WAF1/CIP1} and p16^{INK4A} of glomeruli were shown to be negative (Fig. 6I, 6N), making it difficult to assess their status of senescence *in vivo*.

Renal cortex is much more affected to age-related pathology than renal medulla, so it is better to use the cells from cortex to study the change related to senescence (38). Because proximal tubular epithelial cells are the most abundant in the renal cortex, it is good to use them when examining the phenotype of senescence (39).

In these backgrounds, there is a need to explore the common senescent phenotype of renal proximal tubular cells in both human and animals.

Need for establishment of assay system of cellular senescence

To observe the Hayflick's limit to assess replicative senescence, it takes long time. So the establishment of assay systems that detect renal cellular senescent phenotype within a short period has also been needed. To induce the cells into senescent status by chemical inducer is of great use, though the mechanism of chemically induced senescence and replicative senescence may not be identical.

There are many reports using etoposide, known as an anticancer agent whose mechanism is the inhibition of topoisomerase II, as chemical senescence inducer (40-43), though the mechanism inducing senescence is not clarified. In these reports, many features that prove the senescent status were tested as I also did in my experiments, and treatment with etoposide to cells was thought to be enough to bring cells into senescent status.

Materials and Methods

Cell culture

Primary human renal proximal tubular epithelial cells (RPTECs), derived from 27-year-old Caucasian

female, purchased from Clonetics (Walkersville, MD, USA) were cultured with renal epithelial basal medium (REBM) added with REGM Single-Quots supplement (Clonetics, Walkersville, MD, USA). When comparing cells of early passage and those of late passage, those of passage 3 and 10 were used. Cells of passage 3-4 were used for transfection experiment. Subconfluent (80 % confluence) RPTECs monolayers were passaged at 1:4 split ratio after incubation in Ca²⁺- and Mg²⁺- free, EDTA-containing trypsin solution for 5 minutes. Each experiment with RPTECs was carried out three or more times independently.

Senescence-Associated β -Galactosidase (SABG) staining assay

SABG staining, one of the senescent markers, was performed using Cellular Senescence Assay Kit (Chemicon International, Temecula, CA, USA). Cells were cultured in the 10cm dish. Cells were washed with phosphate-buffered saline (PBS), and fixed with freshly prepared fixing solution (0.5% glutaraldehyde), and incubated at room temperature for 10minutes. After removal of the fixing solution, cells were washed with PBS twice. The freshly prepared SABG detection solution was added on the dish. Cells were incubated at 37°C without CO₂ and protected from the light, for 5 hours. After removal of the solution, cells were washed by PBS twice, and count the blue-stained cells out of total cells under phase contrast microscopy so as to measure the SABG positive rate at the x100 magnification. Ten areas were randomly selected from each group for quantification.

For tissue staining, frozen sections of kidney of 15 μ m were mounted onto glass slides and fixed and stained as same as described in the cellular staining. After staining, counter staining was made with hematoxylin solution, and measure the blue area out of whole cortex so as to calculate the SABG

positive rate at the x100 magnification. Calculation of SABG positive rate of tissue was done using NIH Image J software (National Institutes of Health, Bethesda, MD) with the adequate setting of threshold and computed measurement of area fraction which was obtained after analyzing particles. Eight areas of each kidney section were measured for statistical assessment. Positive rate was expressed as fold increase compared with the levels of young wild type.

Transfection

cDNA of human GLO1 (555bp) was obtained using primers as following; 5'- CAG GCT AGC CAT GGC AGA ACC GCA GCC -3' (forward), 5'- GGA GAA TTC TCA CAG CAC TAC ATT AAG -3' (reverse). Plasmid vector pcDNA3.1(-) (Invitrogen, Carlsbad, CA, USA) was used for overexpression of GLO1. GLO1 containing pcDNA3.1(-) was constructed by inserting the complete human form GLO1 cDNA into the EcoRI and Nhe1 site (Fig. 1A). For overexpression experiments, 400 ng/cm² of GLO1-containing vector or empty vector was transfected into RPTECs for 5 hours incubated with Lipofectamine 2000 (Invitrogen, Carlsbad, CA, USA) according to the manufacturer's instructions, and replaced the culture medium to DMEM with 5% FCS without antibiotics. After the additional incubation for 19 hours, cells were exposed with 1µM of etoposide for 24 hours if necessary. Transfection efficiency was confirmed by the transfection of LacZ-containing vector and then the cells were stained with in situ β galactosidase staining solution according to the manufacturer's protocol with the control using empty vector.

Knockdown study

Knockdown study was performed using Stealth Select RNAi which was purchased from Invitrogen

(Carlsbad, CA, USA). Sequences for GLO1 were as following; 5'- UUA GCG UCA UUC CAA GAA CUC UAG U -3' (siRNA 1), 5'- AAU CCA GUA GCC AUC AGG AUC UUG A -3' (siRNA 2). Stealth RNAi negative control (universal negative control siRNA) from Invitrogen was used as scramble siRNA. 100pmol/cm² of each siRNA was used for knockdown with Lipofectamine 2000 according to the manufacturer's instructions. Knockdown efficiency was confirmed by the quantitative real-time PCR with primers of human GLO1.

RNA isolation and quantitative real-time PCR

1µg of RNA was isolated with Isogen from Nippon Gene (Tokyo, Japan) and reverse-transcribed with Im-Prom II from Promega (Madison, WI) with random primers following the manufacturer's instructions. cDNA was subjected to quantitative real-time PCR using iQ SYBR Green PCR supermix (Bio-Rad Laboratories Inc., Hercules, CA, USA) and the iCycler PCR system.

The primers used for quantitative real-time PCR are as follows; human GLO1 5'- ATT CGG TCA TAT TGG AAT TGC -3' (forward), 5'- TTC AAT CCA GTA GCC ATC AGG -3' (reverse), human p53 5'- CCT CAC CAT CAT CAC ACT GG -3' (forward), 5'- TCT GAG TCA GGC CCT TC TGT -3' (reverse), human p21^{WAF1/CIP1} 5'- TGG AGA CTC TCA GGG TCG AAA -3' (forward), 5'- GGC GTT TGG AGT GGT AGA AAT C -3' (reverse), human p16^{INK4A} 5'- CAA CGC ACC GAA TAG TTA CG -3' (forward), 5'- AGC ACC ACC AGC GTG TC -3' (reverse), human β-actin 5'- TCC CCC AAC TTG AGA TGT ATG AAG -3' (forward), 5'- AAC TGG TCT CAA GTC AGT GTA CAG G -3' (reverse), rat p53 5'- CCT CAA TAA GCT GTT CTG CC -3' (forward), 5'- AAA AGT CTG CCT GTC GTC CA -3' (reverse), rat p21^{WAF1/CIP1} 5'- ACG TGG CCT TGT CGC TGT CTT -3' (forward),

5'- TAA GGC AGA AGA TGG GGA AGA G -3' (reverse), rat p16^{INK4A} 5'- ACG AGG TGC GGG CAC TG -3' (forward), 5'- TTG ACG TTG CCC ATC ATC ATC -3' (reverse), rat β -actin 5'- CTT TCT ACA ATG AGC TGC GTG -3' (forward), 5'- TCA TGA GGT AGT CTG TCA GG -3' (reverse).

Amplification specificity was verified by agarose gel electrophoresis of the PCR products. Expression data were normalized to β -actin using the $\Delta\Delta$ Ct method.

Cell viability test

Cell viability was evaluated with MTS assay and lactate dehydrogenase (LDH) assay. The number of viable cells was determined by using the colorimetric MTS assay using CellTiter 96 AQueous One Solution Cell Proliferation Assay (Promega, Madison, WI, USA). In each well of 96-well plate, 1000 cells of early or late passage with or without etoposide were seeded with REBM, and incubated for 24 hours. Add 10 μ L MTS reagent in 50 μ L cultured media for 1 hour. Thereafter, the 96-well plate was placed into a spectrophotometric plate reader and the absorbance at 492 nm of the content of each well was measured. This measurement was repeated in the day 2, 4 and 6.

Cell viability was also evaluated by LDH assay. 10000 cells of early or late passage with or without etoposide were seeded in to each well of 24-well with REBM, and incubated 24 hours. Cells were lysed with 0.1% Triton X, and 2 μ L of cell lysate and 200 μ L of culture medium were used for each measurement. LDH activity was measured using LDH Kainos (Kainos Laboratories, Tokyo, Japan) according to manufacturer's instruction. LDH release was calculated by determining the ratio of LDH in the culture medium compared with that in the lysed cells plus the culture medium. Release ratio was expressed as a percentage.

γ-glutamyl transpeptidase (GTP) staining

γ-GTP staining was done according to the method described by Rutenburg et al (44). Concisely, cells were washed by PBS twice and reacted with staining solution containing γ-glutamyl-4-melthoxy-2-naphthylamide (GMNA) (0.125mg/mL) added with glycylglycine (0.5mg/mL) and fast blue diazotide 4'-amino-2',5'-diethoxybenzanilide (BBN) (0.5mg/mL). Duration of incubation for staining was 10 minutes at room temperature. No fixation was done before staining.

Chemical analysis

Creatinine concentration was measured by the enzyme method using Cre Kainos (Kainos Laboratories, Tokyo, Japan). Protein concentration was measured by Lowry method using DC Protein Assay Reagents (Bio-Rad Laboratories, Inc. Hercules, CA, USA). Blood or urine sample were used after centrifugation for 5 minutes at 3000 x g. Blood glucose level was measured using an automatic blood glucose meter (Glutest Ace; Sanwa Chemical, Nagoya, Japan).

Determination of GLO1 activity and GSH concentration

Renal cortex of rat (30mg) or 10^4 - 10^5 RPTECs were homogenized in 0.5 mL or 50 μL of NaPB, pH 7.0, containing 0.02% Triton X-100, respectively, and then sonicated for 1 minute and centrifuged at 20,000 x g for 1 minute at 4°C. The supernatant was used for assessment of GLO1 activity by spectrophotometry according to the method noted elsewhere (45), in which the increase in absorbance at 240 nm due to the formation of S-D-lactoylglutathione was monitored for 90 seconds at 25°C. GSH concentration in the renal cortical homogenates from rats was measured with Bioxytech GSH-412 Assay reagent (Oxis International, Portland, OR, USA) according to manufacturer's instruction. The

values were adjusted by the protein concentration of the same sample.

Determination of total superoxide dismutase (SOD) activity

Total SOD activity in renal tissue was determined using superoxide dismutase assay kit (Cayman Chemical, Ann Arbor, MI, USA). Sample preparation and measurement were done according to manufacturer's instruction. Concisely, renal tissues were homogenized in cold 20mM HEPES (pH 7.2), 1mM EGTA, 210mM mannitol, 70mM sucrose per gram tissue. Then they were centrifuged at 1,500 x g for 5 minutes at 4°C. Supernatant fluid was used for assay. The values were adjusted by the protein concentration of the same sample.

Urinary 8-OHdG analysis

Spot urine were collected from rats of each group, and then centrifuged for 10 minutes at 20,000 x g and 4 °C. Supernatants were used for the analysis of 8-OHdG using high sensitive ELISA kit (KOG-HS10/E; Japan Institute for the Control of Aging Co., Ltd, Shizuoka, Japan) according to the manufacturer's instruction. The same urine sample were also used for the measurement of creatinine concentration so as to adjust the concentration of urinary 8-OHdG to daily urinary output.

Immunoblot analysis

Protein solution was made in the condition that 10^4 - 10^5 cells were immersed in 30-300µl urea lysis buffer (8M urea, 10% glycerol, 1% SDS, 10mM Tris-HCl (pH 6.8), 5mM DTT) for cultured cells, or 30mg of minced renal cortex were immersed in 500µl of TG lysis buffer (TritonX 1%, Glycerol 10%, HEPES 20mM, NaCl 100mM) for tissues, and homogenized and sonicated for 1 minute, and then incubated on ice for 30 minutes. Both lysis buffers contain 1T of protease inhibitors (Complete Mini;

Roche, Indianapolis, IN, USA) per 10mL. The samples were subjected to centrifugation at 15,000 x g for 10 minutes at 4°C. The protein concentration of collected supernatant was measured by BCA protein assay kit (Bio-Rad Laboratories Inc., Hercules, CA, USA). The lysates were further denatured by incubation for 5 minutes at 95 °C in sample buffer (2% SDS, 10% glycerol, 60 mM Tris (pH 6.8), 5% β-mercaptoethanol, 0.01% bromophenol blue). The proteins were separated by 10-15% sodium dodecyl sulfate polyacrylamide gel electrophoresis under reduced conditions and transferred onto a PVDF membrane. Monoclonal mouse anti-p53 IgG (1:100; Ab-1, Calbiochem, Cambridge, MA, USA), monoclonal mouse anti-p16^{INK4A} IgG (1:200; sc-1661, Santa Cruz Biotechnology, Santa Cruz, CA, USA), monoclonal mouse anti-4-HNE (15 µg/mL; HNEJ-2, Japan Institute for the Control of Aging Co., Ltd, Shizuoka, Japan) and monoclonal mouse anti-CEL IgG (1:100; given from Ryoji Nagai), polyclonal rabbit anti-β actin IgG (1:1000; A2066, Sigma-Aldrich, St Louis, MO, USA) were used as primary antibodies, and horseradish peroxidase-conjugated anti-mouse or anti-rabbit IgG (1:1000; 170-6516 for anti-mouse, 170-6516 for anti-rabbit, Bio-Rad Laboratories Inc., Hercules, CA, USA) were used as secondary antibodies. The ECL plus Western blotting system (GE Healthcare, Piscataway, NJ, USA) was used for detection. The reproducibility was confirmed in three times of independent experiments, and representative data were presented as figures.

Immunohistochemistry

Sections of 4µm thickness from tissues fixed with methyl Carnoy's were used for the detection of GLO1, p53, p21^{WAF1/CIP1} and p16^{INK4A}. Antigen retrieval was performed by incubating sections for 5 minutes in 10mM citrate buffer in a microwave oven. Polyclonal rabbit anti-GLO1 (25 µg/ml, obtained

from immunization against synthetic peptide of rat GLO1, GIAVPDVYEA , which cross-reacts with human GLO1 epitope, GIAVPDVYSA), anti-p53, monoclonal mouse anti-p21^{WAF1/CIP1}, anti-p16^{INK4A} IgG (1:50 each; sc-6243 for anti-p53, sc-6246 for anti-p21^{WAF1/CIP1}, sc-1661 for anti-p16^{INK4A}, Santa Cruz Biotechnology, Santa Cruz, CA, USA) were used as primary antibodies, and polyclonal horse biotinylated anti-mouse IgG antibody (1:400, BA-2001, Vector Laboratories, Burlingame, CA, USA) or polyclonal goat anti-rabbit IgG (1:400, BA-1000, Vector Laboratories, Burlingame, CA, USA) was used as secondary antibody dissolved in PBS containing 1% bovine serum albumin. Detection of the signal was made with horseradish peroxidase- avidin D (1:2000, A-2004, Vector Laboratories, Burlingame, CA, USA) and diaminobenzidine (1tab/50ml; 045-22833, Wako Chemicals, Osaka, Japan). Specimen were counterstained with hematoxylin. The reproducibility was confirmed in three independent experiments, with representative data presented in results.

Immunofluorescence study

Cells grown on coverslips were washed in PBS, and fixed in 50% methanol/ 50% acetone for 10 minutes at -20°C. The cells were then incubated with PBS containing 1% bovine serum albumin for 1 hour, and incubated with anti-CEL antibody (1:100; KNH-30, TransGenic Inc., Kobe, Japan) as a primary antibody for overnight at 4°C, then FITC-conjugated polyclonal rabbit anti mouse IgG (1:20; F0261, DAKO, Glostrup, Denmark) was used as a secondary antibody following incubation for 1 hour at room temperature. Nuclui were then counterstained with Hoechst33258 (0.05 µg/mL; B2883, Sigma-Aldrich, St Louis, MO, USA). Positivity was determined by comparison with the intensity of sample treated without primary antibody.

Animal experimental protocol

All experiments were conducted in accordance with the Guide for Animal Experimentation at the University of Tokyo. Male Wistar rats (Nippon Seibutsu Zairyo Center, Saitama, Japan) and transgenic Wistar rats overexpressing human GLO1 (GLO1 Tg), generated as described previously (27, 46), were used at the age of 10 weeks and 14 months (each group n=6). GLO1 gene was inserted in the rabbit β -globin downstream of chicken β -actin promoter and CMV enhancer (CAG enhancer-promoter system) (Fig. 1B). They were fed with standard Oriental MF diet (Oriental Yeast Co., Tokyo, Japan) and tap water ad libitum. Food intake was monitored from the 2 weeks before sacrifice and body weight was measured at the time of sacrifice. Systolic blood pressure of awake rats was measured by tail-cuff method using Softron BP-98A (Softron Inc., Tokyo, Japan).

Histological analysis for age-related morphological change

Tissues from rat and human kidney were fixed in formalin solution and paraffin-embedded. Sections of 3 μ m thickness were stained with Masson's trichrome staining for rat, and with Azan staining for human. Interstitial thickness was measured at a magnification of x600 by the distance of blue area that was perpendicularly enclosed with two intact tubules in a manner that the distance became the smallest. Twenty sites selected randomly from 6 fields of renal cortex were used for calculation of interstitial thickness.

Human renal biopsy specimen obtained from the patients admitted to the University of Tokyo Hospital were reviewed with permission and informed consent. Exclusion criteria included confounding factors such as proteinuria (urinary protein > 1 g/gCr), renal dysfunction (estimated glomerular filtration rate

(eGFR) < 60ml/min/1.73m²), interstitial nephritis of primary or secondary origin and diabetes mellitus.

The human renal biopsy specimen were mainly from the patients of IgA nephropathy, and the comparison of glomerular change was neglected because the glomerular change depended on the activity of the disease. Number of recruited patients was 22. Mean GFR was 80.4mL/min/1.73m² (\pm SD 3.48), and mean urinary protein excretion was 0.760 g/day (\pm SD 0.212).

Statistical analysis

All data analyses were performed with Excel 2003 software (Microsoft, Seattle, WA, USA). Data are expressed as mean \pm S.D. Statistical differences were assessed using unpaired Student's t-test or single-factor ANOVA. If significant difference was determined in ANOVA, post hoc comparison (Tukey's method) was made. Values of $P < 0.05$ were considered statistically significant. In the analysis of human renal biopsy, the slope of interstitial thickness against age was calculated by linear regression analysis with Spearman's correlation coefficient.

Results

Validation of etoposide-induced cellular senescence in primary cultured tubular cells

To validate the status of renal senescence, I assessed cellular senescent status by measuring positive rate in SABG staining and expression levels of cell cycle regulators such as p53, p21^{WAF1/CIP1} and p16^{INK4A} in primary cultured human RPTECs at the early and late passages. Cell proliferation estimated by the MTS assay was observed in the early-passaged RPTECs (passage 3), but not observed in the late-passaged cells (passage 10) (Fig. 2A). When the early-passaged cells were treated

with 1 μ M of etoposide, a chemical senescence inducer, the cell growth was inhibited so that the cell number remained the same as the initial condition, which was similar to those observed in the late-passaged cells (Fig. 2A). LDH assay demonstrated no significant differences in cell viability in all three groups (Fig. 2B). In order to eliminate possibility of the transformation from proximal tubular cells to others, the activity of γ -GTP, the specific marker of proximal tubular cells, was evaluated by γ -GTP staining. The activities of tubular cells of all groups were confirmed to be positive, whereas that of rat renal fibroblasts was negative (Fig. 2C).

I then assessed the change in expression levels of cellular senescent markers in RPTECs with different passages and with or without etoposide treatment. The number of SABG positive cells was significantly increased in the late-passaged RPTECs and the early-passaged RPTECs treated with etoposide as compared with untreated early-passaged cells, demonstrating the negative correlation between cell growth and senescent marker expression (Fig. 2D, 2E). To confirm this phenomenon, I further assessed the changes of other senescent markers in these three groups of RPTECs.

Transcriptional level of p53, p21^{WAF1/CIP1} and p16^{INK4A} was significantly increased in RPTECs of late passage or those with etoposide treatment of early passage as compared with the untreated RPTECs at early passage (Fig. 2F). Immunoblot analysis followed by densitometry revealed the upregulation of p53 of whole cellular lysate at the protein level in RPTECs in association with growth arrest (Fig. 2G). There were no good antibodies available for the detection of human p21^{WAF1/CIP1} and p16^{INK4A} in this assay system. The amount of CEL, an indicator of the accumulated AGEs, was examined by immunofluorescent microscopy. Cells of late passage and those with etoposide exposure presented

positive signals, whereas those of early passage did not (Fig. 2H).

Beneficial effect of GLO1 on senescence of tubular cells

Next, I utilized RPTECs treated with etoposide for functional studies. First, I performed gain-of-function studies by utilizing the early-passaged RPTECs overexpressing human GLO1 which is a detoxifying enzyme of reactive carbonyls thereby implicated in senescence. I confirmed that the transfection efficiency in RPTECs estimated by LacZ expression as a reporter gene was about 90 %, and the GLO1 activity was upregulated by about 6 times in GLO1-transfected cells compared with empty-vector-transfected cells (Fig. 3A). Overexpression of GLO1 did not change the basal expression level of SABG in these transfectants. Of note, the empty-vector-transfected cells treated by etoposide showed an increase in SABG-positive cells by approximately 50%, it was significantly suppressed by GLO1 overexpression (Fig. 3B, 3C). Transcript expression levels of p53, p21^{WAF1/CIP1} and p16^{INK4A}, and protein expression level of p53 of whole cellular lysate stimulated with etoposide were also significantly decreased in GLO1-transfected cells as compared with the empty vector-transfected cells, whereas those without etoposide did not have the significant differences (Fig. 3D, 3E, 3F). And the accumulation of CEL detected by immunofluorescence augmented by etoposide was significantly suppressed by GLO1 overexpression, whereas it was remained increased with transfection of empty vector (Fig. 3G).

I also performed loss-of-function experiments using siRNA targeted to human GLO1. Knockdown efficiency of siRNA1 and siRNA2 estimated by quantitative RT-PCR was 93% and 94%, respectively (Fig. 4A). The GLO1 activity was inhibited by approximately 60 % by the knockdown (Fig. 4B). Of

note, when GLO1-knocked down cells were treated with etoposide, the number of positive cells for SABG staining was significantly increased as compared with those in control siRNA-transfected cells (Fig. 4C, 4D). Other senescent markers, such as transcript expression level of p53, p21^{WAF1/CIP1} and p16^{INK4A}, or protein expression level of p53 of whole cellular lysate, were also markedly augmented by knockdown of GLO1 (Fig. 4E, 4F, 4G). These gain and loss of function studies of GLO1 on RPTECs suggested that GLO1 has the cytoprotective effect against renal tubular senescence.

The age-related morphological change in interstitium of human kidney

I then assessed the age-related morphological change of human renal senescence, especially focusing on the tubulointerstitial changes. Reviewing specimen from 22 patients stained with Azan-staining, whose renal function were preserved (eGFR mean $80.4 \pm \text{S.D. } 3.48 \text{ mL/min./1.73m}^2$, urinary protein excretion mean $0.760 \pm \text{S.D. } 0.212 \text{ g/day}$), the thickness of interstitium was changed according to age (Fig. 5B). Linear regression analysis showed excellent positive Spearman's correlation coefficient between age and thickness of renal peritubular interstitium (slope $0.044\mu\text{m/year}$, $r^2 = 0.91$, $p < 0.01$).

Validation of senescent status in aged kidney

I then compared senescent status in the kidney of young (10-week-old) and elderly (14-month-old) rats. Systolic blood pressure was not significantly different between two groups (young wild type: 106 ± 2.6 , elderly wild type $104 \pm 11 \text{ mmHg}$, mean \pm S.D.), nor blood glucose levels of two groups were (Fig. 6A in WT). Serum creatinine and urinary protein excretion were significantly elevated in elderly rats compared with young rats (Fig. 6G, 6H in WT). Elevated serum creatinine level in elderly rats might reflect the decreased renal function.

As to pathological senescence phenotype observed in human kidney, kidney from elderly rats showed marked tubulointerstitial thickening compared with the kidney from young (Fig. 6I, 6J in WT). And also more positive area of renal cortex in SABG staining was observed in elderly rats than in young rats (Fig. 6K, 6L in WT). Immunohistochemistry and quantitative real-time RT-PCR analysis for detection of senescent markers p53, p21^{WAF1/CIP1} and p16^{INK4A} showed that these expressions in the kidney of the elderly were significantly increased compared with those of the young, and immunoblot analysis for detection of p53, p16^{INK4A}, CEL in renal cortex also showed that these expressions in the elderly were significantly increased compared with those of the young as I expected (Fig. 6M, 6N, 6O, 6P, 6Q in WT). Taken together with the results of senescence studies *in vitro* using RPTECs of late passage suggested that increased expression of senescent markers such as SABG, p53, p21^{WAF1/CIP1}, p16^{INK4A} and CEL reflected renal senescence phenotype including cellular growth arrest and pathological change of tubulointerstitium.

Amelioration of senescent phenotype in aged-kidney of GLO1 transgenic rats

In order to assess a biological role of GLO1 on renal senescence *in vivo*, I used the GLO1 transgenic rats of young and elderly compared with those of wild type (46). Wistar strain was adopted in both GLO1 transgenic and wild type rats. Body weight was not significantly different between the groups of the same age (young wild type: 320 ± 15, young GLO1-Tg: 330 ± 28, elderly wild type 470 ± 47, elderly GLO1-Tg: 460 ± 30 g/rat, mean ± S.D.). Food intake per body weight was not significantly different in all groups (young wild type: 44 ± 13, young GLO1-Tg: 42 ± 14, elderly wild type 40 ± 13, elderly GLO1-Tg: 44 ± 14 mg/day/g rat weight, mean ± S.D.). Systolic blood pressure was also not

significantly different in all groups (young wild type: 106 ± 2.6 , young GLO1-Tg: 105 ± 5.7 , elderly wild type 104 ± 11 , elderly GLO1-Tg: 102 ± 7.6 mmHg, mean \pm S.D.). Blood glucose levels were not significantly different between the transgenic and wild type rats during the experimental period (Fig. 6A). The concentration of GSH, a cofactor of GLO1, which affects the activity of GLO1, was not different in renal cortex between young and aged rats of GLO1-Tg and wild type (Fig. 6B). The GLO1 activity showed about 6 times increase as high in GLO1-Tg rats as wild type animals (Fig. 6D), as consistent with the previous report (46). In wild type rats, its activity was significantly decreased by age to approximately half (Fig. 6C). In contrast, no significant changes by aging were observed in GLO1-Tg rats (Fig. 6D). GLO1 was ubiquitously expressed in kidney of both young and elderly rats, and in GLO1 transgenic rats glomerular and tubular epithelial predominance was observed (Fig. 6E), which is consistent with the feature of the CAG enhancer - promoter system.

To eliminate the effect of antioxidants, which may lead to ameliorate the senescent phenotypes by reduction of ROS, I measured the renal SOD activity, which is a representative antioxidant enzyme. Total SOD activity was measured, which includes cytosolic SOD1, mitochondrial SOD2, and extracellular SOD (SOD3). The enzymatic activity was not statistically changed by GLO1 overexpression at the age of both young and elderly (Fig. 6F). Serum creatinine level, which correlates inversely with renal function, and protein excretion from kidney, both of which were increased in the elderly of wild type, were significantly suppressed by overexpression of GLO1 (Fig. 6G, 6H). Importantly, tubulointerstitial morphological phenotype of renal senescence observed in both aged kidney of wild type rats and human renal biopsies was significantly reduced in GLO1-Tg rats of the

elderly (Fig. 6I, 6J). The histological improvement against renal senescence was associated with a decrease in SABG expression level; the kidney of aged GLO1-Tg rats had less SABG positive rate than that in the wild type rats of the same age (Fig. 6K, 6L). No significant differences were observed between the kidneys of young experimental animals of GLO1-Tg and wild type. Elevated transcript levels of p53, p21^{WAF} and p16^{INK4A} of the aged rats were significantly suppressed by GLO1 overexpression compared with those of wild type, whereas no significant differences were observed in both young groups (Fig. 6M). Immunohistochemistry for senescent markers p53, p21^{WAF} and p16^{INK4A} showed that nuclei of renal cortical tubules of aged wild type rats were stained positive, and that these levels of positive staining were markedly reduced in GLO1-Tg rats when they were aged (Fig. 6N). The similar results were obtained by immunoblot analysis for p53 and p16^{INK4A} of whole lysate of renal cortex; protein expression level of p53 or p16^{INK4A} in young experimental animals was undetectable, however, increased expressions of p53 and p16^{INK4A} by age were reduced by GLO1 overexpression (Fig. 6O, 6P). And parallelly, accumulation of AGEs in renal cortex, detected by the immunoblot for CEL, which was elevated by aging, was markedly suppressed by overexpression of GLO1, whereas no significant changes were observed in both young rats (Fig. 6Q).

Overexpression of GLO1 ameliorates oxidative stress in aged kidney

The level of oxidative stress in kidney was also assessed by measurement of urinary 8-OHdG concentration and immunoblot analysis of whole lysate of 4-HNE of renal cortex. There were significant increases in both urinary 8-OHdG concentration and protein modification by 4-HNE in aged wild type rats than those of younger ones, and their age-dependent increases were significantly

suppressed by overexpression of GLO1. (Fig. 6R, 6S)

Discussion

To think the senescence of the organ which composes of many kinds of cells, there is a problem what cell is the most appropriate for assessment of senescent phenotype. I chose the tubular epithelial cells as assaying target of senescence. In the previous experiment *in vivo*, age-related morphological change of tubulointerstitial area was observed even in the absence of the age-related changes in glomeruli such as glomerulosclerosis (data not shown). So tubular (or tubulointerstitial) change may be of good indicator of senescent status, which turns to be positive in early stage of senescence. This may reflect that the difference of metabolic rates of cells, considering the evidence that podocytes, endothelial cells or cells other than tubular cells have far less number of mitochondria than epithelial tubular cells.

In cells treated with etoposide, senescence was induced within the short period, but the senescent phenotype may be somewhat different from that of replicative senescence observed in late passages. However, I confirmed up-regulation of CEL accumulation and other various senescent markers in RPTECs treated with etoposide, so it is plausible and justified to use etoposide in the experiments on cellular senescence.

The baseline (background) level of the SABG positive rate in each experiment was different. These differences may be due to the cytotoxicity of vector or siRNA and/or transfection reagent.

In SABG staining and immunohistochemical studies *in vivo*, not all the tubular cells were positive. This may imply that the renal tubular cells do not acquire the senescent phenotype at the same rate.

Considering that the morphological change was observed more extensively than senescent markers, this may be due to either of the following possibilities. First, the difference of sensitivity of SABG staining or antibody used in immunohistochemistry. The level of antigen expression may depend on segments of tubules. Second, the existence of circulating factors excreted from senescent-marker-positive cells to induce morphological senescence. Further study may reveal the precise mechanism.

In this study, we verified age-related phenotypes of kidney *in vitro* utilizing primary cultured tubular cells and chemical senescence-inducer etoposide and studies *in vivo* utilizing rat and human aged kidney. The results showed that the premature senescence induced by etoposide can serve as an appropriate model of replicative senescence in primary cultured tubular cells, and these senescence phenotypic changes were correlated with pathological senescence changes such as tubulointerstitial thickening in association of renal dysfunction both in humans and rats. Importantly, these renal senescence phenotypic changes observed in studies *in vitro* and *in vivo* were significantly altered by GLO1, which is an enzyme to detoxify the carbonyl stress including MG, highly reactive and pathogenic AGE precursor and thereby reduce AGE formation; GLO1 overexpression ameliorated the senescence of tubular cells while GLO1 knockdown enhanced, and aged kidney overexpressing GLO1 suppressed the pathological senescence phenotypes associated with renal dysfunction. These studies for the first time demonstrated the characterization of senescence phenotypes in the kidney and a crucial role of GLO1 in the renal senescence.

My finding that the GLO1 attenuates renal senescence by decreasing AGE formation is consistent

with the previous studies. For example, cultured endothelial cells subjected to AGE-modified collagen type I developed premature senescence (47). Mice given low-dose D-galactose showed deposition of AGEs and progressive ultrastructural aging in retinal pigment epithelium with the similar changes of the transcriptome to the generalized aging response (48). Taken together with the findings that aged kidney shows an increase of AGE accumulation in association with a decrease in GLO1 activity (Fig. 6C) as shown in aged human lens (49), in aged human red blood cells (45), and in aged human brain (50, 51), acceleration of AGE-formation with age may induce, at least in part, renal senescence, thereby GLO1 reduces the senescence phenotype via inhibition of AGE formation. To support my hypothesis, a recent report showed that overexpression of GLO1 homologue CeGly induces the longevity of *C.elegans* (11), In contrast, mice fed a diet with a lowered content of AGEs did not increase oxidative stress or kidney fibrosis with aging (52). This discrepancy may be explained by the different influence to the senescence between AGEs formed in situ and AGEs intake from the food.

Accumulating evidence has demonstrated that oxidative stress is involved in the aging process. Longevity achieved by caloric restriction or deficiency in angiotensin type 1 receptor is associated with low levels of ROS production (10). And overexpression of Klotho, an anti-aging gene, showed a reduction in superoxide anion generation and lipid peroxidation in association with renoprotective effects (53). However, contrary to my expectation, there are few definite reports that overexpression of direct ROS-eliminating enzymes induce longevity or less phenotype of aging. While overexpression of human catalase targeted to mitochondria extended the life-span about 20% in the mice (9), ectopic or entopic overexpression of catalase did not (8). Overexpression of SOD1 or SOD2 also failed to extend

the life-span of mice (7, 8). One possible explanation is that excessive reduction of ROS may cancel out its beneficial effects as ROS also plays a pivotal role in various physiological processes (12). And dicarbonyl adducts and AGEs are generated as by-products of ROS generation through glycooxidation. From this viewpoint, it is suggested that AGEs are more appropriate targets than ROS in terms of aging researches.

I used primary cultured RPTECs in studies *in vitro*, and they reached the status of replicative senescence at a relatively early passage (approximately passage 10) as compared with other primary cultured cells such as fibroblasts (approximately passage 40). This is consistent with the previous report (54). These phenomena might reflect the rapid turn over, short life-span when cultured on the dish or their nature of high-differentiation.

Kidney excretes AGEs, so it can be the target for AGE-induced injury. Analysis of the InCHIANTI study in Italy showed that plasma CML was an independent predictor of decline in renal function in aged community-dwelling adults (55). Therefore, the enhancement of decomposition of AGEs may naturally have good effect on renal senescence. And my preliminary study showed that the aorta of the aged GLO1-Tg rats showed less phenotype of senescence compared with aged wild type rats (data not shown), suggesting that my findings in the kidney can be generalized to other organs or a whole organism. And based on these findings, the discovery of new drugs which enhance GLO1 activity may reduce the age-related disease or prevent from aging.

Mechanism of progression of renal senescence or deterioration of renal function by AGEs still remained to be elucidated. One possible mechanism is that sustained cytotoxic effects of AGEs or

precursors of AGEs such as MG formed in situ change the renal cells, especially of high metabolic rates such as tubular cells, into low-turnover or senescent cells with fibrogenic circumstances. Another possibility is that the circulating AGEs stimulate the renal cells through AGE receptors such as RAGE etc. And it is also possible that not only extracellular matrix but also cell cycle regulators are the target of glycation, which may let the cells into more senescent status than apoptotic status. The glycation of extracellular matrix such as collagen and fibronectin in kidney may lead to depositional tendency to kidney so as to incur the interstitial thickening.

Reduced renal function (GFR) due to chronic kidney disease is usually explained by the glomerular damage, so that the glomerulus has long been the target of study on chronic kidney disease. Because of inability to assess the glomerular senescent status and my preliminary observation that no morphological changes implying reduced GFR such as glomerulosclerosis were found in the aged rat kidney used in my experiments, I focused my attention to tubulointerstitium. Interstitial thickening itself may explain the reduced GFR by the increased vascular resistance or reduced number of nephrons, which can not be assessed by the observation of microscopy if the glomeruli are morphologically intact. The precise mechanism still remained to be elucidated.

Disclosure

Reviewing human specimen of renal biopsy was performed with permission of the ethics committee of Graduate School of Medicine, University of Tokyo, and informed consent from patients were obtained previously.

(Permission No. 2671)

Acknowledgments

I am grateful to my mentors, Dr. Masaomi Nangaku, Dr. Reiko Inagi and Prof. Toshiro Fujita (the University of Tokyo) for their supervision during the long time of my doctoral course. I would like to express great thanks to my lab member, especially Takanori Kumagai, Tetsuhiro Tanaka for technical advices and Prof. Toshio Miyata (Tohoku University) and Ryoji Nagai (Japan Women's University) for their material supply.

References

1. Dimri, GP, Lee, X, Basile, G, Acosta, M, Scott, G, Roskelley, C, Medrano, EE, Linskens, M, Rubelj, I, Pereira-Smith, O, Peacocke, M & Campisi, J: A biomarker that identifies senescent human cells in culture and in aging skin in vivo. *Proc Natl Acad Sci U S A*, 92: 9363-7, 1995.
2. Duncan, EL, Wadhwa, R & Kaul, SC: Senescence and immortalization of human cells. *Biogerontology*, 1: 103-21, 2000.
3. Vasile, E, Tomita, Y, Brown, LF, Kocher, O & Dvorak, HF: Differential expression of thymosin beta-10 by early passage and senescent vascular endothelium is modulated by VPF/VEGF: evidence for senescent endothelial cells in vivo at sites of atherosclerosis. *Faseb J*, 15: 458-66, 2001.
4. Choi, J, Shendrik, I, Peacocke, M, Peehl, D, Buttyan, R, Ikeguchi, EF, Katz, AE & Benson, MC: Expression of senescence-associated beta-galactosidase in enlarged prostates from men with benign prostatic hyperplasia. *Urology*, 56: 160-6, 2000.
5. Harman, D: Aging: a theory based on free radical and radiation chemistry. *J Gerontol*, 11: 298-300, 1956.
6. Bordone, L & Guarente, L: Calorie restriction, SIRT1 and metabolism: understanding longevity. *Nat Rev Mol Cell Biol*, 6: 298-305, 2005.
7. Perez, VI, Bokov, A, Remmen, HV, Mele, J, Ran, Q, Ikeno, Y & Richardson, A: Is the oxidative stress theory of aging dead? *Biochim Biophys Acta*, 1790: 1005-14, 2009.
8. Perez, VI, Van Remmen, H, Bokov, A, Epstein, CJ, Vijg, J & Richardson, A: The overexpression of major antioxidant enzymes does not extend the lifespan of mice. *Aging Cell*, 8: 73-5, 2009.
9. Schriener, SE, Linford, NJ, Martin, GM, Treuting, P, Ogburn, CE, Emond, M, Coskun, PE, Ladiges, W, Wolf, N, Van Remmen, H, Wallace, DC & Rabinovitch, PS: Extension of murine life span by overexpression of catalase targeted to mitochondria. *Science*, 308: 1909-11, 2005.
10. Benigni, A, Corna, D, Zoja, C, Sonzogni, A, Latini, R, Salio, M, Conti, S, Rottoli, D, Longaretti, L, Cassis, P, Morigi, M, Coffman, TM & Remuzzi, G: Disruption of the Ang II type 1 receptor promotes longevity in mice. *J Clin Invest*, 119: 524-30, 2009.
11. Morcos, M, Du, X, Pfisterer, F, Hutter, H, Sayed, AA, Thornalley, P, Ahmed, N, Baynes, J, Thorpe, S, Kukudov, G, Schlotterer, A, Bozorgmehr, F, El Baki, RA, Stern, D, Moehrlen, F, Ibrahim, Y, Oikonomou, D, Hamann, A, Becker, C, Zeier, M, Schwenger, V, Miftari, N, Humpert, P, Hammes, HP, Buechler, M, Bierhaus, A, Brownlee, M & Nawroth, PP: Glyoxalase-1 prevents mitochondrial protein modification and enhances lifespan in *Caenorhabditis elegans*. *Aging Cell*, 7: 260-9, 2008.
12. Finkel, T & Holbrook, NJ: Oxidants, oxidative stress and the biology of ageing. *Nature*, 408: 239-47, 2000.
13. Stadtman, ER: Protein oxidation and aging. *Science*, 257: 1220-4, 1992.
14. Nagai, R, Fujiwara, Y, Mera, K, Motomura, K, Iwao, Y, Tsurushima, K, Nagai, M, Takeo, K,

- Yoshitomi, M, Otagiri, M & Ikeda, T: Usefulness of antibodies for evaluating the biological significance of AGEs. *Ann N Y Acad Sci*, 1126: 38-41, 2008.
15. Nagai, R, Fujiwara, Y, Mera, K, Yamagata, K, Sakashita, N & Takeya, M: Immunochemical detection of Nepsilon-(carboxyethyl)lysine using a specific antibody. *J Immunol Methods*, 332: 112-20, 2008.
 16. Uribarri, J, Cai, W, Peppas, M, Goodman, S, Ferrucci, L, Striker, G & Vlassara, H: Circulating glycotoxins and dietary advanced glycation endproducts: two links to inflammatory response, oxidative stress, and aging. *J Gerontol A Biol Sci Med Sci*, 62: 427-33, 2007.
 17. Munch, G, Shepherd, CE, McCann, H, Brooks, WS, Kwok, JB, Arendt, T, Hallupp, M, Schofield, PR, Martins, RN & Halliday, GM: Intraneuronal advanced glycation endproducts in presenilin-1 Alzheimer's disease. *Neuroreport*, 13: 601-4, 2002.
 18. Ahmed, N: Advanced glycation endproducts--role in pathology of diabetic complications. *Diabetes Res Clin Pract*, 67: 3-21, 2005.
 19. Chen, J, Huang, X, Halicka, D, Brodsky, S, Avram, A, Eskander, J, Bloomgarden, NA, Darzynkiewicz, Z & Goligorsky, MS: Contribution of p16INK4a and p21CIP1 pathways to induction of premature senescence of human endothelial cells: permissive role of p53. *Am J Physiol Heart Circ Physiol*, 290: H1575-86, 2006.
 20. Verzola, D, Gandolfo, MT, Gaetani, G, Ferraris, A, Mangerini, R, Ferrario, F, Villaggio, B, Gianiorio, F, Tosetti, F, Weiss, U, Traverso, P, Mji, M, Deferrari, G & Garibotto, G: Accelerated senescence in the kidneys of patients with type 2 diabetic nephropathy. *Am J Physiol Renal Physiol*, 295: F1563-73, 2008.
 21. Thangarajah, H, Yao, D, Chang, EI, Shi, Y, Jazayeri, L, Vial, IN, Galiano, RD, Du, XL, Grogan, R, Galvez, MG, Januszyk, M, Brownlee, M & Gurtner, GC: The molecular basis for impaired hypoxia-induced VEGF expression in diabetic tissues. *Proc Natl Acad Sci U S A*, 106: 13505-10, 2009.
 22. Inoue, Y & Kimura, A: Identification of the structural gene for glyoxalase I from *Saccharomyces cerevisiae*. *J Biol Chem*, 271: 25958-65, 1996.
 23. Ranganathan, S, Walsh, ES, Godwin, AK & Tew, KD: Cloning and characterization of human colon glyoxalase-I. *J Biol Chem*, 268: 5661-7, 1993.
 24. Cameron, AD, Olin, B, Ridderstrom, M, Mannervik, B & Jones, TA: Crystal structure of human glyoxalase I--evidence for gene duplication and 3D domain swapping. *Embo J*, 16: 3386-95, 1997.
 25. Thornalley, PJ: The glyoxalase system: new developments towards functional characterization of a metabolic pathway fundamental to biological life. *Biochem J*, 269: 1-11, 1990.
 26. Hayes, JD, Milner, SW & Walker, SW: Expression of glyoxalase, glutathione peroxidase and glutathione S-transferase isoenzymes in different bovine tissues. *Biochim Biophys Acta*, 994: 21-9, 1989.
 27. Kumagai, T, Nangaku, M, Kojima, I, Nagai, R, Ingelfinger, JR, Miyata, T, Fujita, T & Inagi, R: Glyoxalase I overexpression ameliorates renal ischemia-reperfusion injury in rats. *Am J Physiol Renal Physiol*, 296: F912-21, 2009.

28. Lindeman, RD, Tobin, J & Shock, NW: Longitudinal studies on the rate of decline in renal function with age. *J Am Geriatr Soc*, 33: 278-85, 1985.
29. Abrass, CK, Adcox, MJ & Raugi, GJ: Aging-associated changes in renal extracellular matrix. *Am J Pathol*, 146: 742-52, 1995.
30. Ruiz-Torres, MP, Bosch, RJ, O'Valle, F, Del Moral, RG, Ramirez, C, Masseroli, M, Perez-Caballero, C, Iglesias, MC, Rodriguez-Puyol, M & Rodriguez-Puyol, D: Age-related increase in expression of TGF-beta1 in the rat kidney: relationship to morphologic changes. *J Am Soc Nephrol*, 9: 782-91, 1998.
31. Ding, G, Franki, N, Kapasi, AA, Reddy, K, Gibbons, N & Singhal, PC: Tubular cell senescence and expression of TGF-beta1 and p21(WAF1/CIP1) in tubulointerstitial fibrosis of aging rats. *Exp Mol Pathol*, 70: 43-53, 2001.
32. Gray, JE, Weaver, RN & Purmalis, A: Ultrastructural observations of chronic progressive nephrosis in the Sprague-Dawley rat. *Vet Pathol*, 11: 153-64, 1974.
33. Gray, JE: Chronic progressive nephrosis in the albino rat. *CRC Crit Rev Toxicol*, 5: 115-44, 1977.
34. Fogo, A & Ichikawa, I: Evidence for a pathogenic linkage between glomerular hypertrophy and sclerosis. *Am J Kidney Dis*, 17: 666-9, 1991.
35. Nyengaard, JR & Bendtsen, TF: Glomerular number and size in relation to age, kidney weight, and body surface in normal man. *Anat Rec*, 232: 194-201, 1992.
36. He, C, Esposito, C, Phillips, C, Zalups, RK, Henderson, DA, Striker, GE & Striker, LJ: Dissociation of glomerular hypertrophy, cell proliferation, and glomerulosclerosis in mouse strains heterozygous for a mutation (Os) which induces a 50% reduction in nephron number. *J Clin Invest*, 97: 1242-9, 1996.
37. Zheng, F, Striker, GE, Esposito, C, Lupia, E & Striker, LJ: Strain differences rather than hyperglycemia determine the severity of glomerulosclerosis in mice. *Kidney Int*, 54: 1999-2007, 1998.
38. Percy, C, Pat, B, Poronnik, P & Gobe, G: Role of oxidative stress in age-associated chronic kidney pathologies. *Adv Chronic Kidney Dis*, 12: 78-83, 2005.
39. Jennette, JC, Olson, J.L., Schwartz, M.M., Silva, F.G.: *Heptinstall's Pathology of the Kidney*, 2007.
40. Krizhanovsky, V, Yon, M, Dickins, RA, Hearn, S, Simon, J, Miething, C, Yee, H, Zender, L & Lowe, SW: Senescence of activated stellate cells limits liver fibrosis. *Cell*, 134: 657-67, 2008.
41. te Poele, RH, Okorokov, AL, Jardine, L, Cummings, J & Joel, SP: DNA damage is able to induce senescence in tumor cells in vitro and in vivo. *Cancer Res*, 62: 1876-83, 2002.
42. Robles, SJ, Buehler, PW, Negrusz, A & Adami, GR: Permanent cell cycle arrest in asynchronously proliferating normal human fibroblasts treated with doxorubicin or etoposide but not camptothecin. *Biochem Pharmacol*, 58: 675-85, 1999.
43. Wang, Y, Blandino, G, Oren, M & Givol, D: Induced p53 expression in lung cancer cell line promotes cell senescence and differentially modifies the cytotoxicity of anti-cancer drugs. *Oncogene*, 17: 1923-30, 1998.
44. Rutenburg, AM, Kim, H, Fischbein, JW, Hanker, JS, Wasserkrug, HL & Seligman, AM:

- Histochemical and ultrastructural demonstration of gamma-glutamyl transpeptidase activity. *J Histochem Cytochem*, 17: 517-26, 1969.
45. McLellan, AC & Thornalley, PJ: Glyoxalase activity in human red blood cells fractioned by age. *Mech Ageing Dev*, 48: 63-71, 1989.
46. Inagi, R, Miyata, T, Ueda, Y, Yoshino, A, Nangaku, M, van Ypersele de Strihou, C & Kurokawa, K: Efficient in vitro lowering of carbonyl stress by the glyoxalase system in conventional glucose peritoneal dialysis fluid. *Kidney Int*, 62: 679-87, 2002.
47. Patschan, S, Chen, J, Polotskaia, A, Mendeleev, N, Cheng, J, Patschan, D & Goligorsky, MS: Lipid mediators of autophagy in stress-induced premature senescence of endothelial cells. *Am J Physiol Heart Circ Physiol*, 294: H1119-29, 2008.
48. Tian, J, Ishibashi, K, Reiser, K, Grebe, R, Biswal, S, Gehlbach, P & Handa, JT: Advanced glycation endproduct-induced aging of the retinal pigment epithelium and choroid: a comprehensive transcriptional response. *Proc Natl Acad Sci U S A*, 102: 11846-51, 2005.
49. Haik, GM, Jr., Lo, TW & Thornalley, PJ: Methylglyoxal concentration and glyoxalase activities in the human lens. *Exp Eye Res*, 59: 497-500, 1994.
50. Kuhla, B, Boeck, K, Luth, HJ, Schmidt, A, Weigle, B, Schmitz, M, Ogunlade, V, Munch, G & Arendt, T: Age-dependent changes of glyoxalase I expression in human brain. *Neurobiol Aging*, 27: 815-22, 2006.
51. Kuhla, B, Boeck, K, Schmidt, A, Ogunlade, V, Arendt, T, Munch, G & Luth, HJ: Age- and stage-dependent glyoxalase I expression and its activity in normal and Alzheimer's disease brains. *Neurobiol Aging*, 28: 29-41, 2007.
52. Cai, W, Gao, QD, Zhu, L, Peppas, M, He, C & Vlassara, H: Oxidative stress-inducing carbonyl compounds from common foods: novel mediators of cellular dysfunction. *Mol Med*, 8: 337-46, 2002.
53. Haruna, Y, Kashihara, N, Satoh, M, Tomita, N, Namikoshi, T, Sasaki, T, Fujimori, T, Xie, P & Kanwar, YS: Amelioration of progressive renal injury by genetic manipulation of Klotho gene. *Proc Natl Acad Sci U S A*, 104: 2331-6, 2007.
54. Glynne, PA: *Primary Culture of Human Proximal Renal Tubular Epithelial Cells*, Totowa, NJ, Humana Press Inc. 1999.
55. Semba, RD, Fink, JC, Sun, K, Bandinelli, S, Guralnik, JM & Ferrucci, L: Carboxymethyl-lysine, an advanced glycation end product, and decline of renal function in older community-dwelling adults. *Eur J Nutr*, 48: 38-44, 2009.

Figure Legends and Figures

Fig.1

(A) GLO1 transgene construct used in the study *in vitro* (GLO1-containing plasmid vector).

(B) GLO1 transgene construct used in the study *in vivo* (GLO1 transgenic rat).

(C) Schematic representation of monomer of GLO1.

(D) Schematic representation of dimer of GLO1.

Fig.2

Validation of renal cellular senescence using RPTECs and etoposide.

(A) Cell proliferation rate determined by MTS assay. Each assay was made every other day. Value of day0 was set as 1. Mean \pm S.D. * $p < 0.01$, ** $p < 0.05$ versus passage 3 of day 0.

(B) LDH release of RPTECs of passage 3 with or without etoposide exposure and passage 10. LDH release was calculated by $(\text{LDH in culture supernatant} / \text{LDH in culture supernatant} + \text{LDH in cell lysate}) \times 100$. Mean LDH release (%) \pm S.D.

(C) Phase-contrast light micrographs with γ -GTP staining of RPTECs of passage 3 with or without etoposide exposure and passage 10 and rat renal fibroblasts. Original magnification $\times 100$. Bar $200\mu\text{m}$. Red cells are positive for γ -GTP activity.

(D) Phase-contrast light micrographs with SABG staining of RPTECs of passage 3 with or without etoposide exposure and passage 10. Original magnification $\times 100$. Bar $200\mu\text{m}$. Blue cells are positive.

- (E) Quantitative analysis of SABG positive cells. Positive cells per total cells in each field. Mean \pm S.D. * $p < 0.01$ versus passage 3 of day 0.
- (F) Relative transcript levels of p53, p21^{WAF1/CIP1} and p16^{INK4A} of RPTECs of passage 3 with or without etoposide exposure and passage 10 determined by quantitative real-time RT-PCR. Each of passage 3 without etoposide was set as 1. Mean \pm S.D. * $p < 0.01$, ** $p < 0.05$ versus each of passage 3, # $p < 0.05$ versus p21^{WAF1/CIP1} of passage 10.
- (G) Protein immunoblot of p53 of whole lysate of RPTECs of passage 3 with or without etoposide exposure and passage 10. Actin was presented as control.
- (H) Immunofluorescent micrographs for the detection of CEL. Green (anti-CEL, FITC). Blue (Hoechst33258). Original magnification x400, Bar 50 μ m.

Fig.3

Overexpression of GLO1 attenuated the senescent phenotype of RPTECs of early passage with etoposide exposure.

- (A) GLO1 activity assay measured after 24h from transfection of each vector. Mean \pm S.D. * $p < 0.01$ versus empty vector.
- (B) Phase-contrast light micrographs with SABG staining of RPTECs transfected with empty vector or GLO1-containing vector with or without etoposide exposure. Original magnification x 100. Bar 200 μ m. Blue cells are positive.
- (C) Quantitative analysis of SABG positive cells. Positive cells per total cells in each field. Mean

± S.D. * p<0.01 versus cells without etoposide transfected with empty vector.

- (D) Relative transcript levels of p53, p21^{WAF1/CIP1} and p16^{INK4A} of RPTECs with etoposide exposure transfected with plasmid vector determined by quantitative real-time RT-PCR. Each of those transfected with empty vector was set as 1. Mean ± S.D. * p<0.01, ** p<0.05 versus each of cells transfected with empty vector.
- (E) Protein immunoblot of p53 of whole lysate of RPTECs with or without etoposide exposure transfected with plasmid vectors. Actin was presented as control.
- (F) Densitometric quantification of p53 immunoblot of RPTECs with or without etoposide exposure transfected with plasmid vectors. Level of those transfected with empty vector without etoposide exposure was set as 1. Mean ± S.D. * p<0.01, ** p<0.05 versus cells without etoposide exposure transfected with empty vector.
- (G) Immunofluorescent micrographs of RPTECs with or without etoposide exposure transfected with plasmid vectors for the detection of CEL accumulation. Green (anti-CEL, FITC). Blue (Hoechst33258). Original magnification x400, Bar 100µm.

Fig.4

Knockdown of GLO1 exacerbated the senescent phenotype of RPTECs of early passage with etoposide exposure.

- (A) Transcript levels of GLO1 determined by quantitative real-time RT-PCR measured after 24h from transfection. Mean ± S.D. * p<0.01 versus control siRNA.

- (B) GLO1 activity assay measured after 24h from transfection of siRNA or control. Mean \pm S.D. * $p < 0.01$ versus empty vector.
- (C) Phase-contrast light micrographs with SABG staining of RPTECs transfected with siRNA or control with etoposide exposure. Original magnification $\times 100$. Bar $200\mu\text{m}$. Blue cells are positive.
- (D) Quantitative analysis of SABG positive cells. Positive cells per total cells in each field. Mean \pm S.D. * $p < 0.05$ versus cells with etoposide transfected with control siRNA.
- (E) Relative transcript levels of p53, p21^{WAF1/CIP1} and p16^{INK4A} of RPTECs with etoposide exposure transfected with siRNA or control determined by quantitative real-time RT-PCR. Each of those transfected with control siRNA was set as 1. Mean \pm S.D. * $p < 0.01$, ** $p < 0.05$ versus each of cells with etoposide transfected with control siRNA.
- (F) Protein immunoblot of p53 of whole lysate of RPTECs with etoposide exposure transfected with siRNA or control. Actin was presented as control.
- (G) Densitometric quantification of p53 immunoblot. Level of those transfected with control siRNA was set as 1. Mean \pm S.D. * $p < 0.05$ versus cells transfected with control siRNA.

Fig.5

Interstitial thickening was demonstrated to be age-related morphological change of human kidney.

- (A) Representative figures of human renal biopsy. Formalin fixed specimen ($3\mu\text{m}$ thick) were Azan stained. Red-stained cells are proximal tubular epithelial cells and blue area interstitia. Original

magnification x 600. Bar 20 μ m.

(B) Correlation between age and interstitial thickness. The univariate linear regression line was drawn.

Each dot represents mean thickness (μ m), and bar represents S.D.(μ m). Calculation method is described in Material and Method.

Fig.6

GLO1 transgenic rats of the elderly presented less senescent phenotype.

(A) Blood glucose levels of each group of rats. Mean \pm S.D.

(B) GSH levels of the lysate of renal cortex of each group of rats. Data were adjusted by protein concentration. Mean \pm S.D.

(C) GLO1 activity of the lysate of renal cortex. Comparison of wild type rats of the young and elderly. Data were adjusted by protein concentration. Mean \pm S.D. * $p < 0.01$

(D) GLO1 activity of the lysate of renal cortex. Comparison of wild type and GLO1 transgenic rats. Data were adjusted by protein concentration. Mean \pm S.D. * $p < 0.01$ versus to young wild type.

(E) Distribution of GLO1 in rat kidney. Representative micrographs of immunohistochemistry staining GLO1 in the rat renal cortex. Methyl Carnoy's fixed specimen (4 μ m thick) were counterstained with hematoxylin. Original magnification x 200. Bar 100 μ m.

(F) Total SOD activity of the lysate of renal cortex of each group of rats. Data were adjusted by protein concentration. Mean \pm S.D.

(G) Serum creatinine levels of each group of rats determined by enzymic assay. Mean \pm S.D. * $p < 0.01$,

** p<0.05.

- (H) Urinary protein excretion of each group of rats. Spot urine was used for measure. Data were adjusted by urinary creatinine concentration. Mean \pm S.D. * p<0.01, ** p<0.05.
- (I) Light micrographs of rat renal cortex. Formalin fixed specimen (3 μ m thick) were stained with Masson's trichrome staining. Red-stained cells with brush borders are proximal tubular epithelial cells and blue area interstitia. Original magnification x 600. Bar 10 μ m.
- (J) Quantification of interstitial thickness. Calculation was made by the same method as an analysis of human renal biopsy. Mean \pm S.D. * p<0.01, ** p<0.05.
- (K) Light micrographs of rat renal cortex with SABG staining. Frozen tissue specimen (15 μ m thick) were from counterstained with Nuclear Fast Red. Original magnification x 100. Bar 100 μ m. Blue cells are positive.
- (L) Quantitative analysis of SABG positive area. Positive rate was calculated by division of positive area by total area in each field. Positive rate was expressed as fold increase compared with the level of young wild type. Mean \pm S.D. * p<0.01.
- (M) Relative transcript levels of p53, p21^{WAF1/CIP1} and p16^{INK4A} determined by quantitative real-time RT-PCR. Each of young wild type rats was set as 1. Mean \pm S.D. * p<0.01, ** p<0.05 versus each of young wild type. # p<0.01 versus each of elderly wild type.
- (N) Representative micrographs of immunohistochemistry staining p53, p21^{WAF1/CIP1} and p16^{INK4A} in the rat renal cortex. Methyl Carnoy's fixed specimen (4 μ m thick) were counterstained with hematoxylin. Original magnification x 400. Bar 50 μ m.

(O) Protein immunoblot of p53 and p16^{INK4A} of the whole lysate of renal cortex. Actin was presented as control.

(P) Densitometric quantification of p53 and p16^{INK4A} immunoblot. Mean \pm S.D. * p<0.05 versus young wild type.

(Q) Protein immunoblot of CEL of whole lysate of rat renal cortex. Actin was presented as control.

Many bands were detected as CEL-modified protein, indicating AGEs were accumulated in renal cortex.

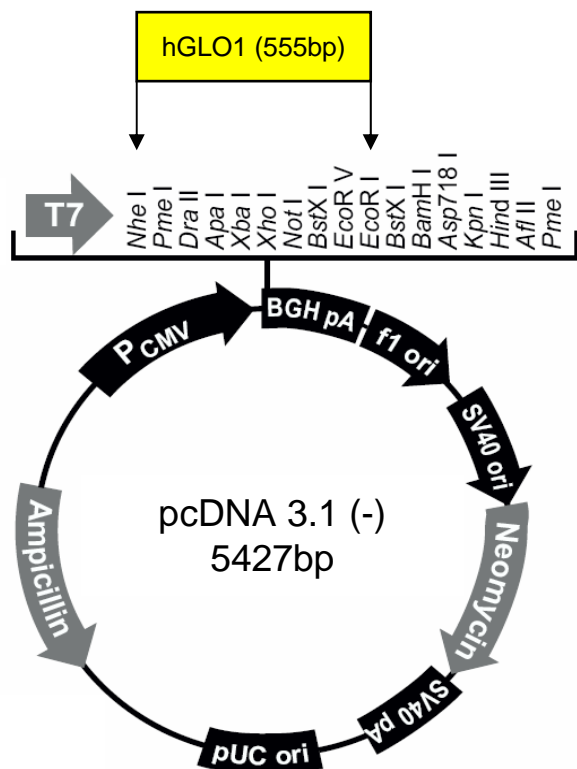
(R) Urinary 8-OHdG levels. Spot urine was used for measure. Data were adjusted by urinary creatinine concentration. Mean \pm S.D. * p<0.01, ** p<0.05.

(S) Protein immunoblot of 4-HNE of whole lysate of rat renal cortex. Actin was presented as control.

Increased number of bands and increased intensity indicated that oxidative stress were elevated.

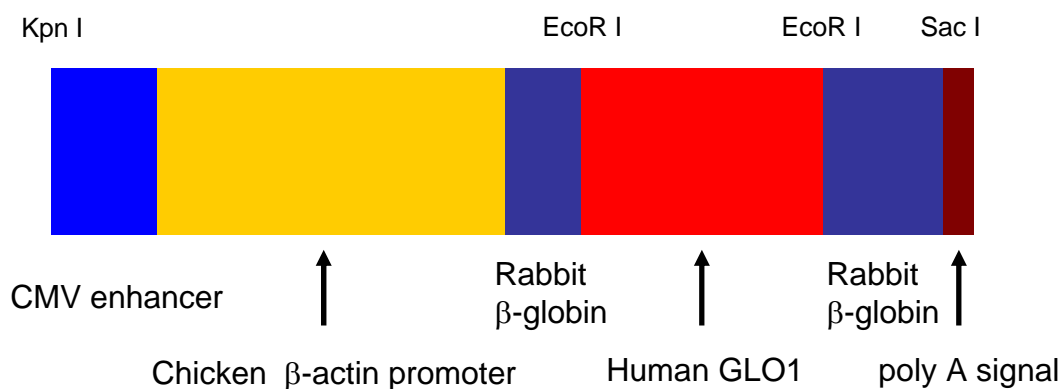
Figure 1

A

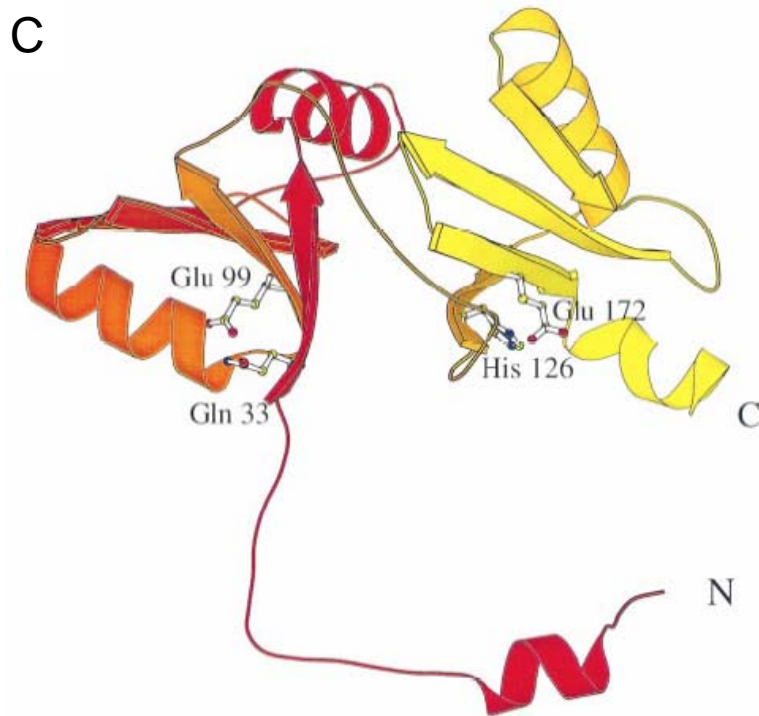


Glyoxalase I (GLO1) transgene construct used in study in vitro (GLO1-containing plasmid vector). Full-length human GLO1 cDNA (555bp) was cloned into pcDNA 3.1(-).

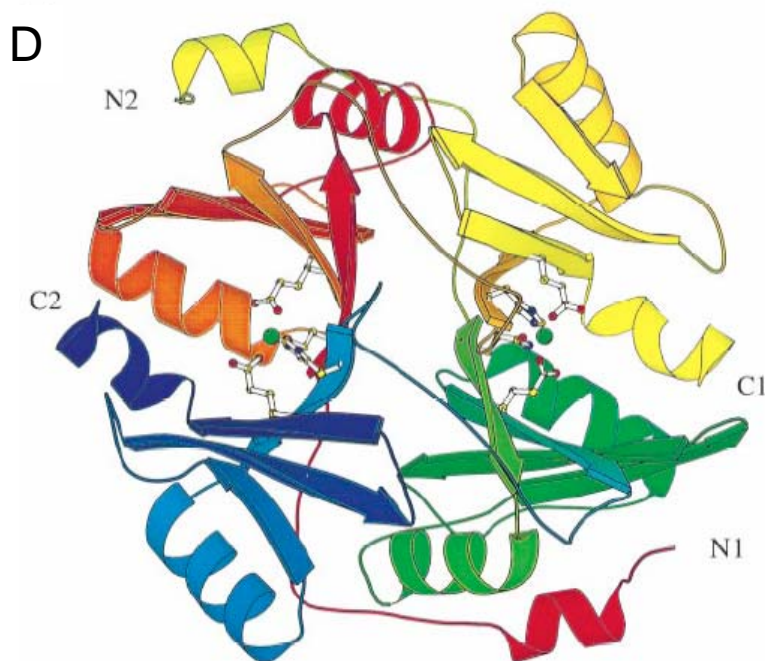
B



GLO1 transgene construct used in study in vivo (GLO1 transgenic rat). Full-length human GLO1 cDNA was cloned in the rabbit β -globin gene including a part of the second intron, the third exon and the 3' untranslated region (39).



Schematic representation of monomer of GLO1 (21).

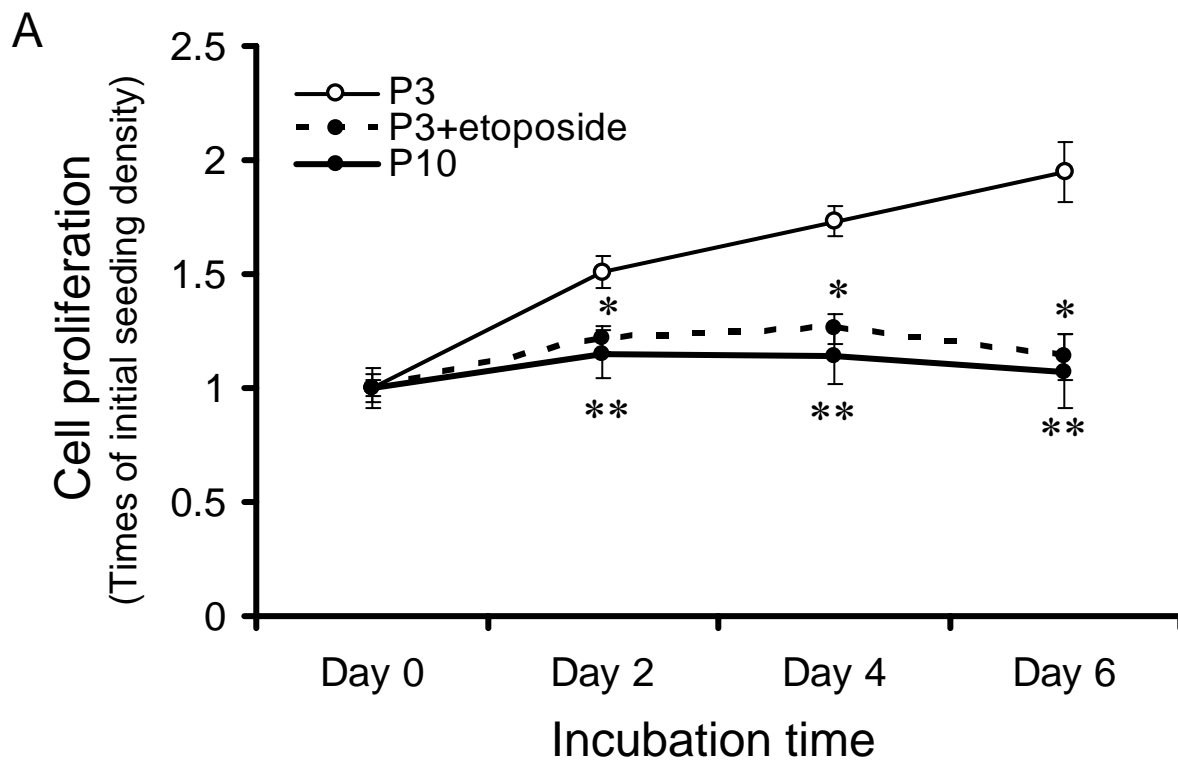


Schematic representation of dimer of GLO1 (21).

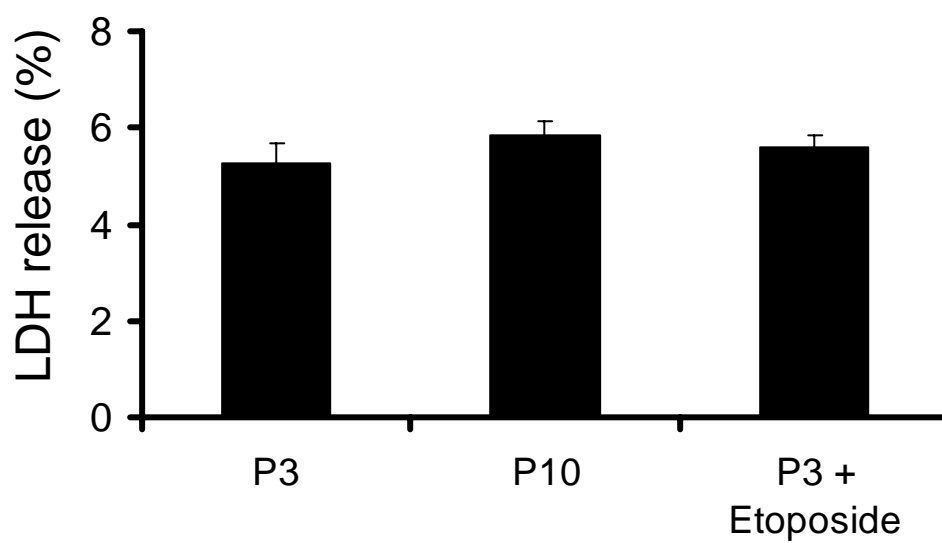
The dimer has been colour ramped according to residue number, starting with red at the N-terminus of one molecule, passing through yellow at the C-terminus of that molecule and finishing with blue at the C-terminus of the other monomer. The zinc and its coordinating residues are shown in a ball and stick representation with the zinc coloured green.

The active sites is situated in a barrel which is formed only on dimerization.

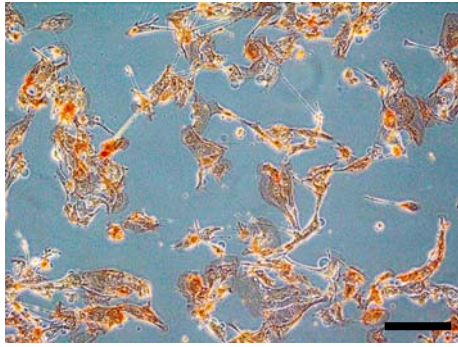
Figure 2



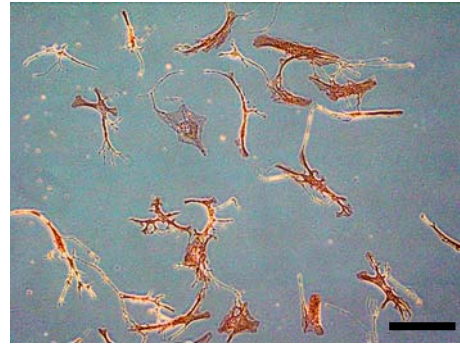
B



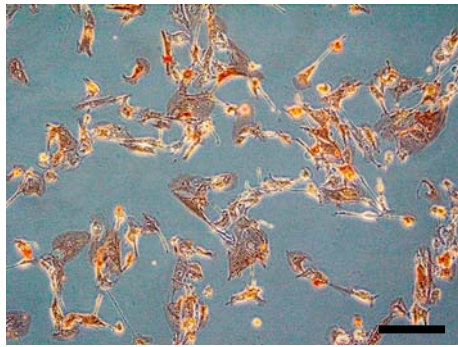
C



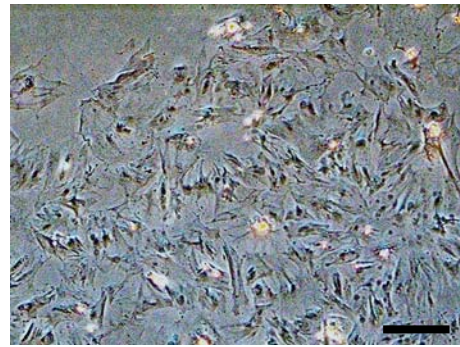
P3



P10

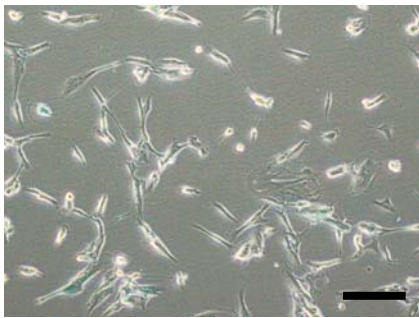


P3 + Etoposide

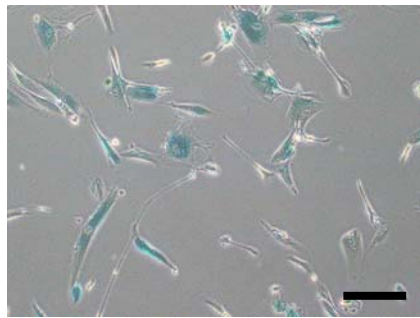


rat renal fibroblasts

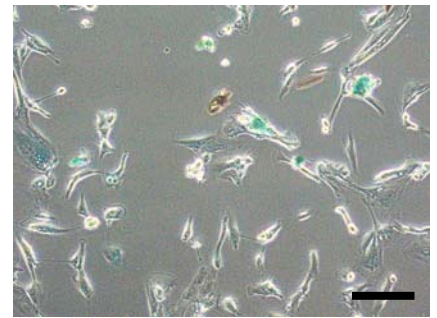
D



P3

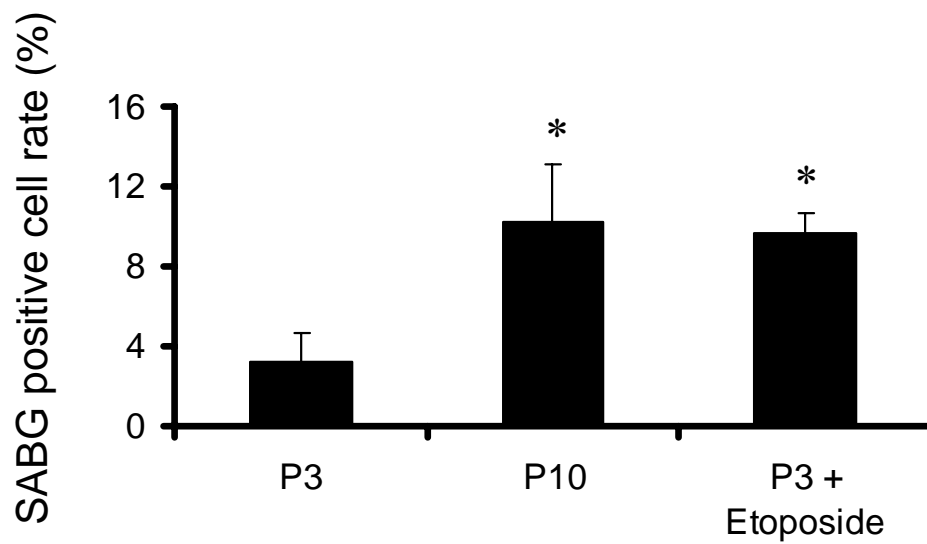


P10



P3 + Etoposide

E



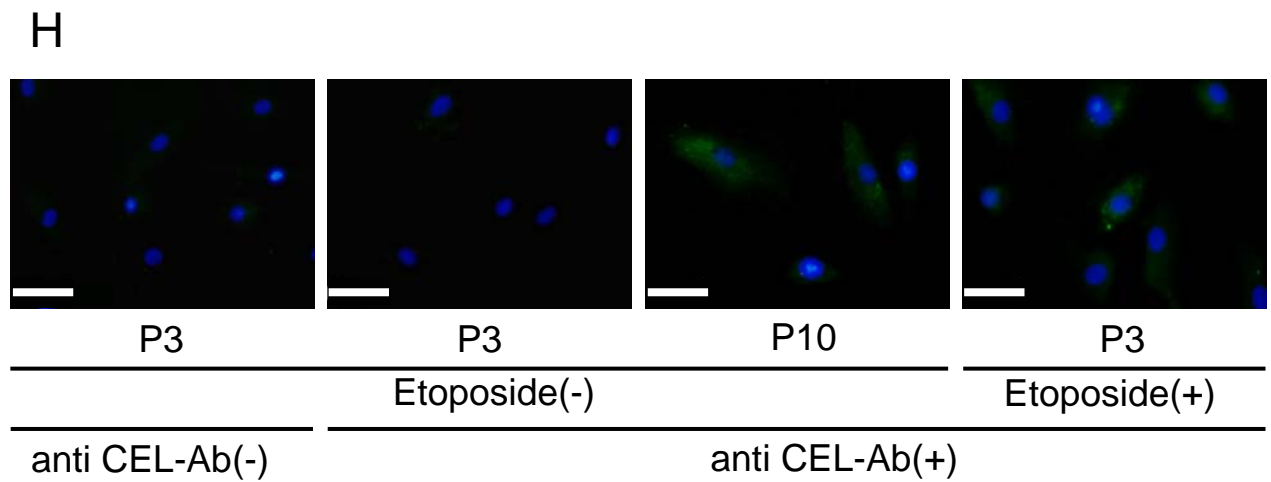
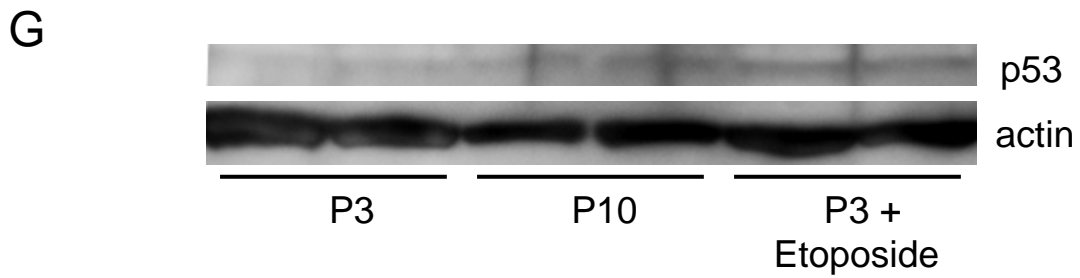
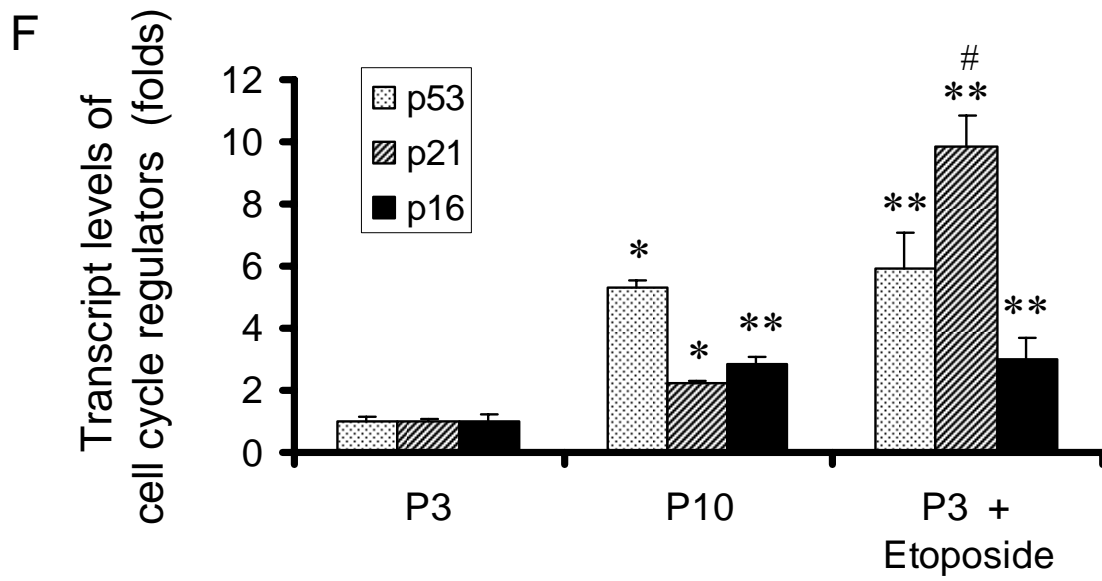
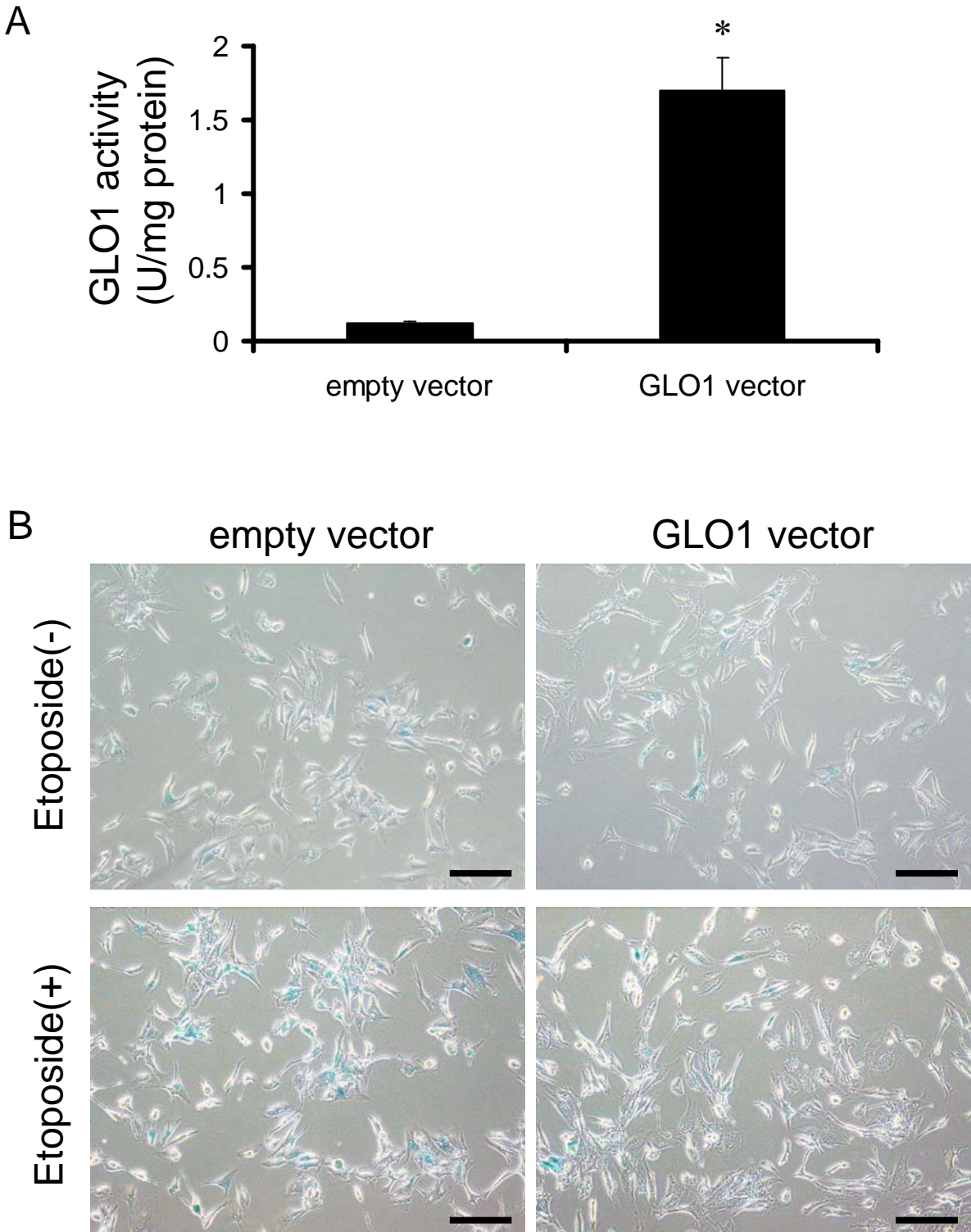
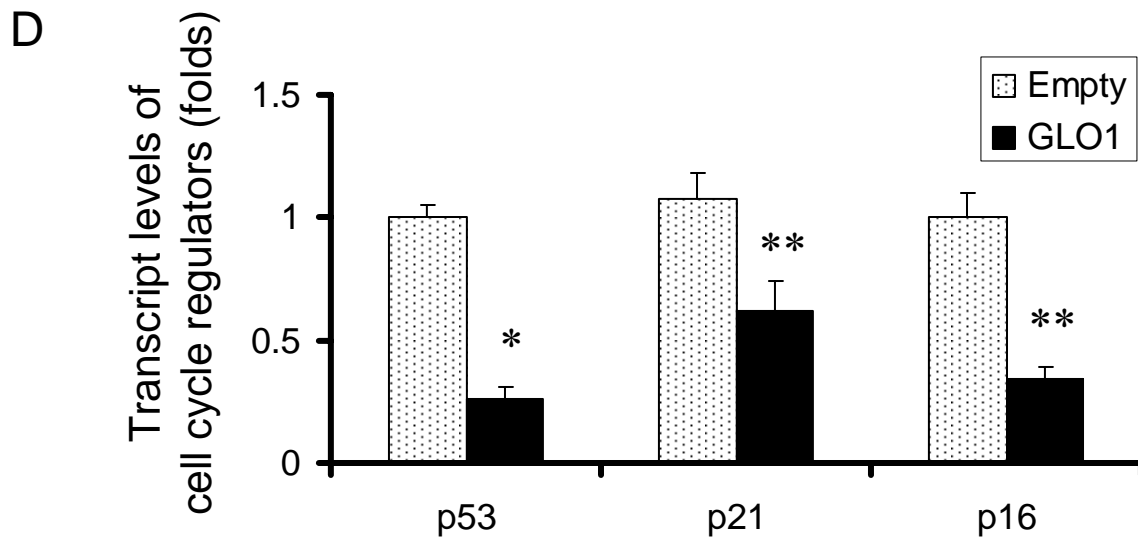
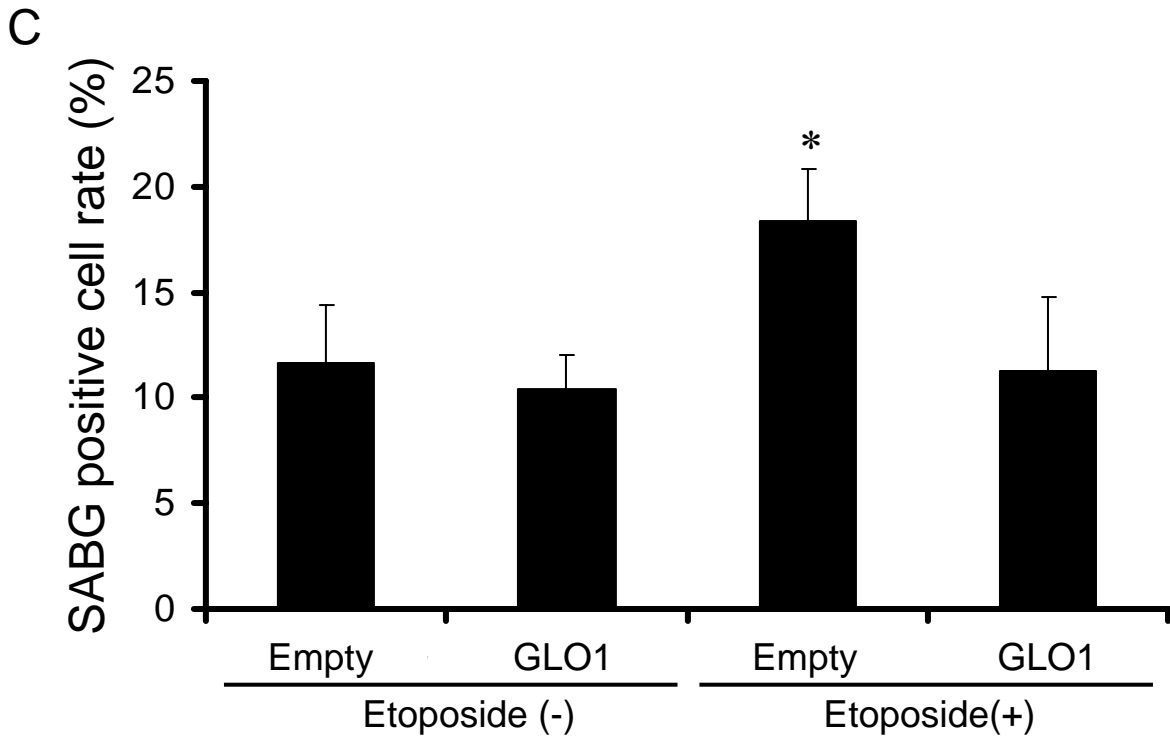
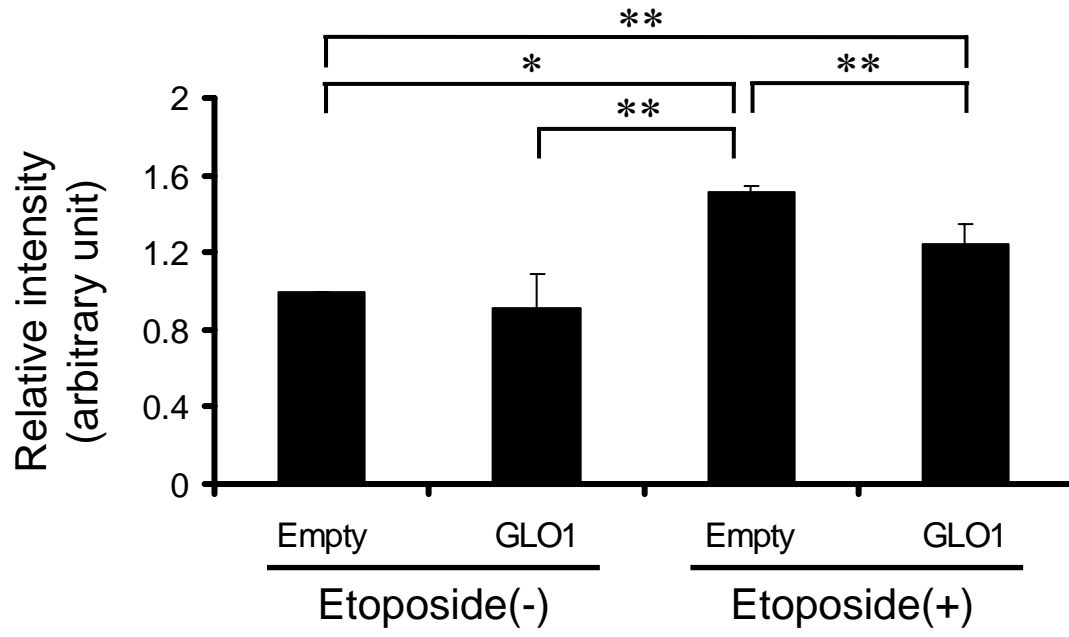


Figure 3





F



G

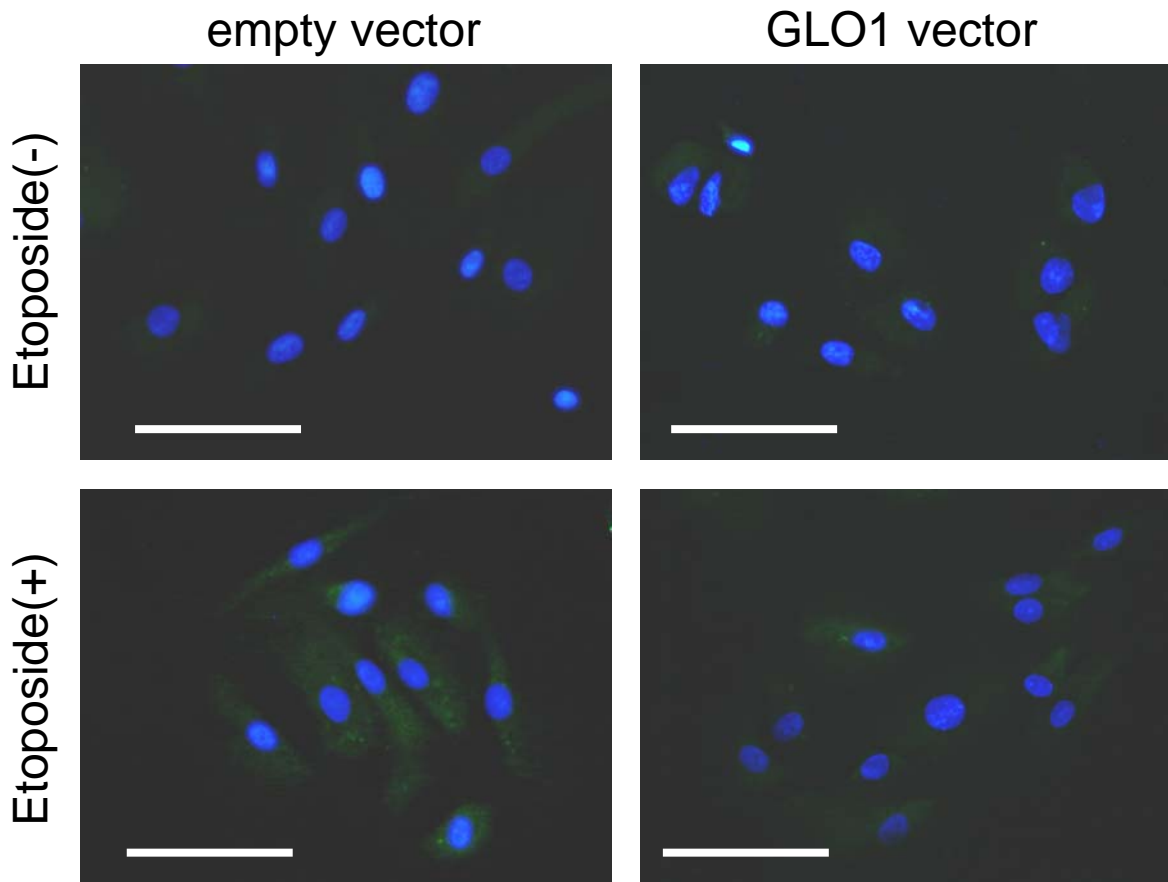
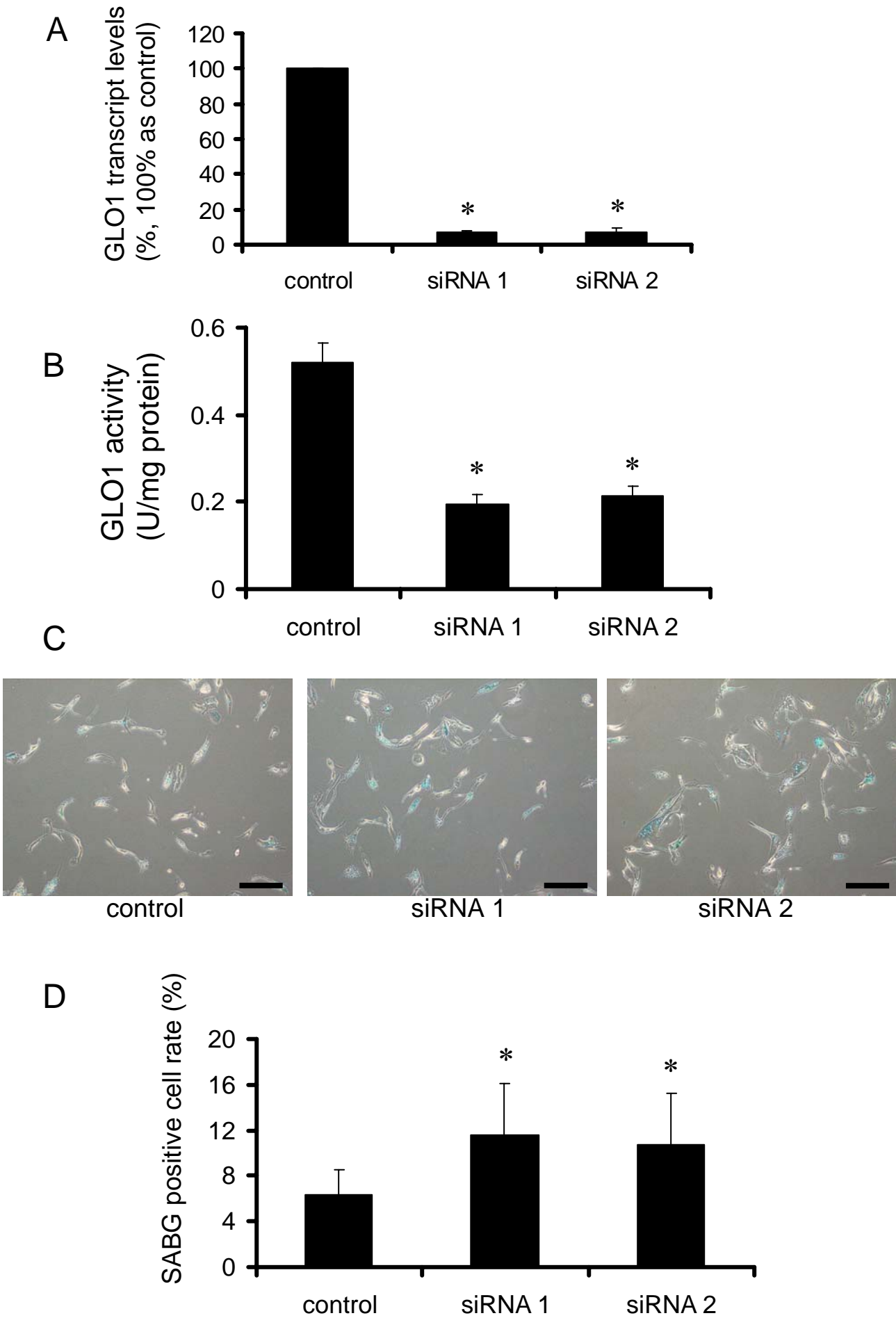


Figure 4



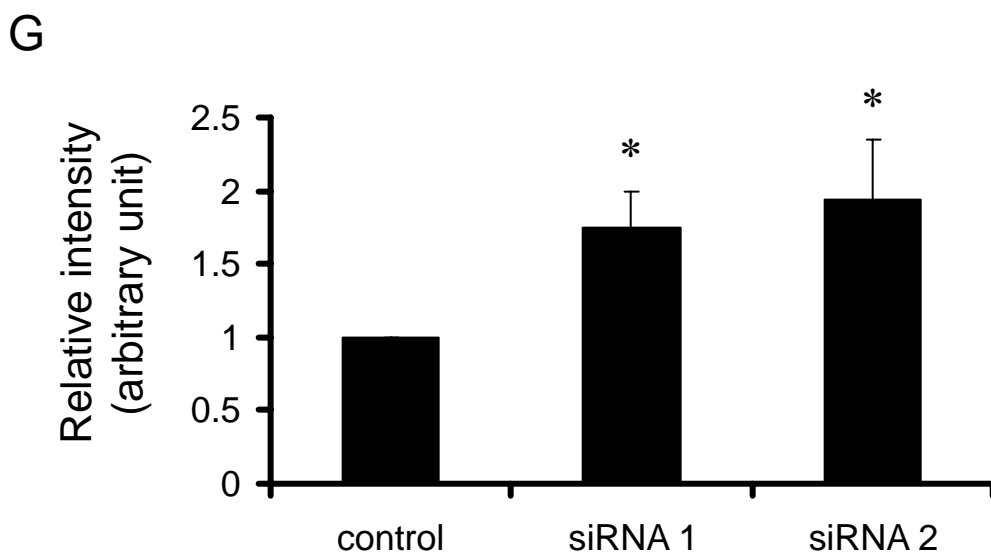
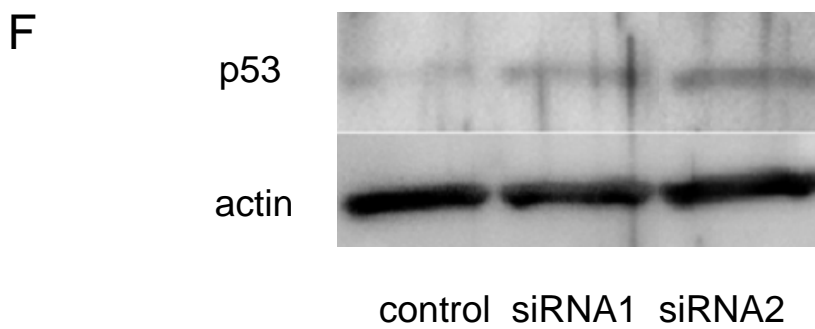
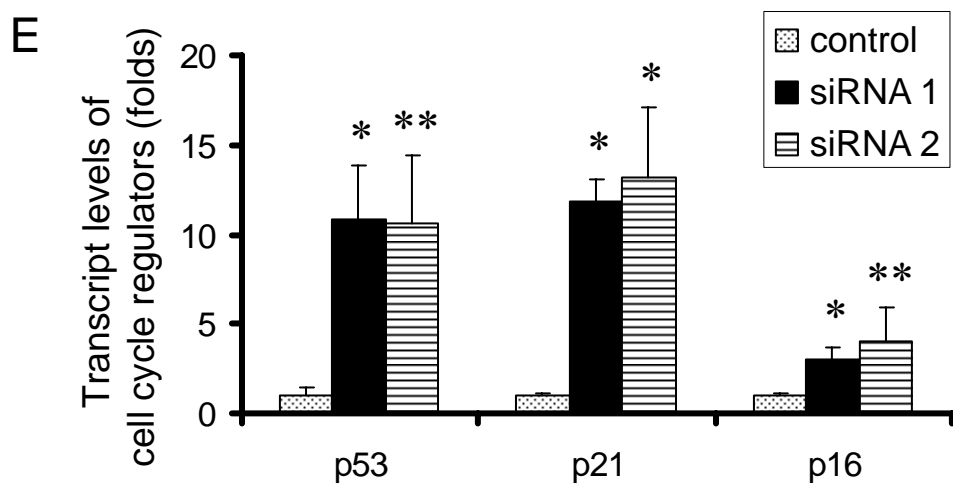
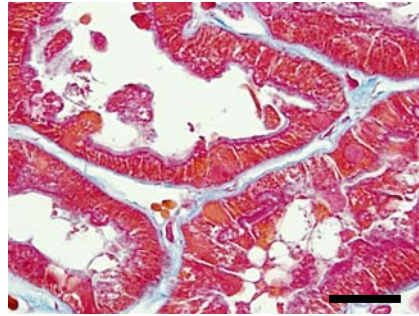
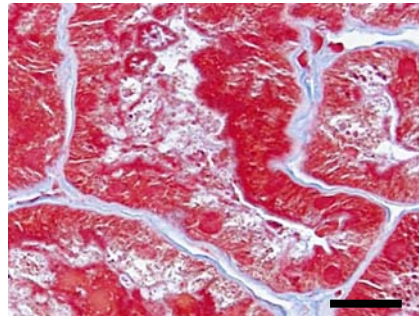


Figure 5

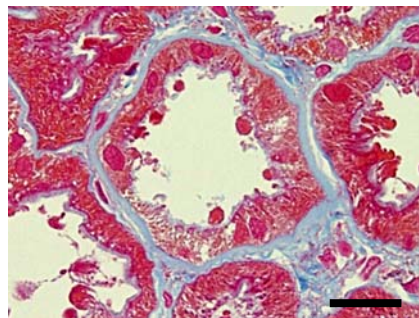
A



32 years old



43 years old



58 years old

B

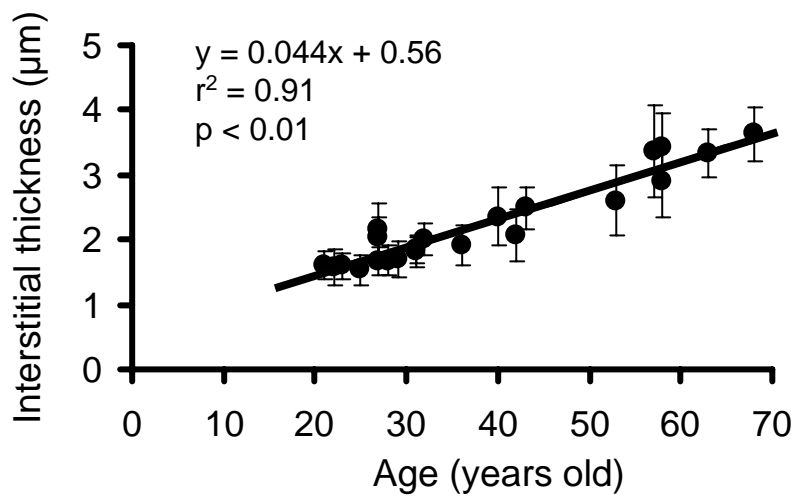
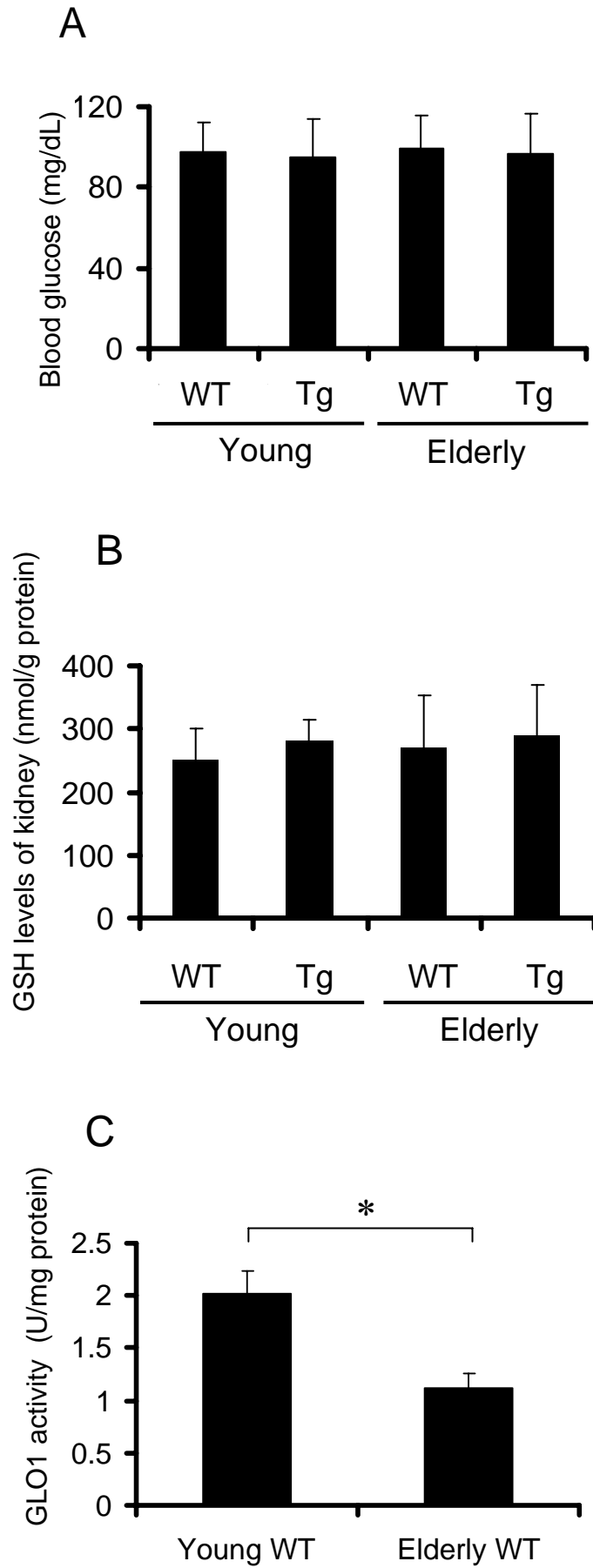
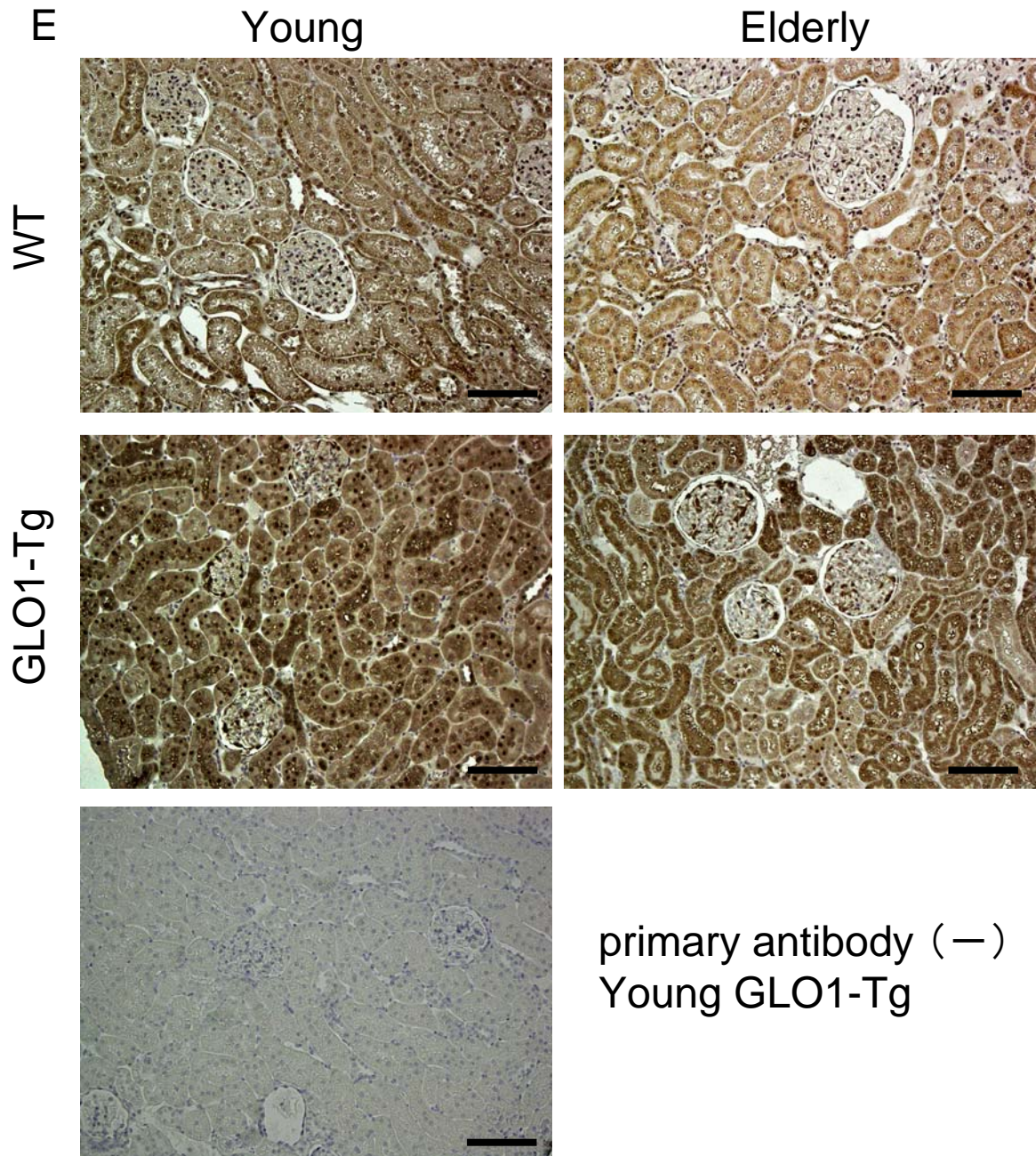
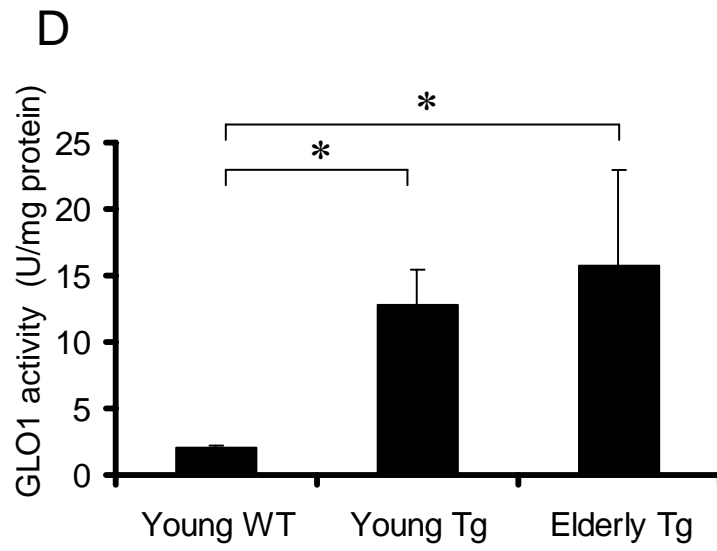
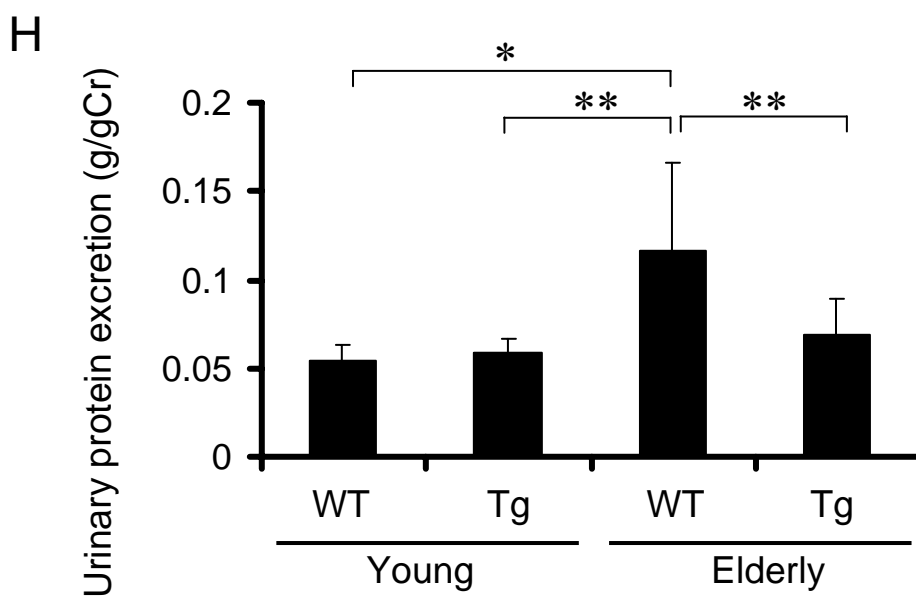
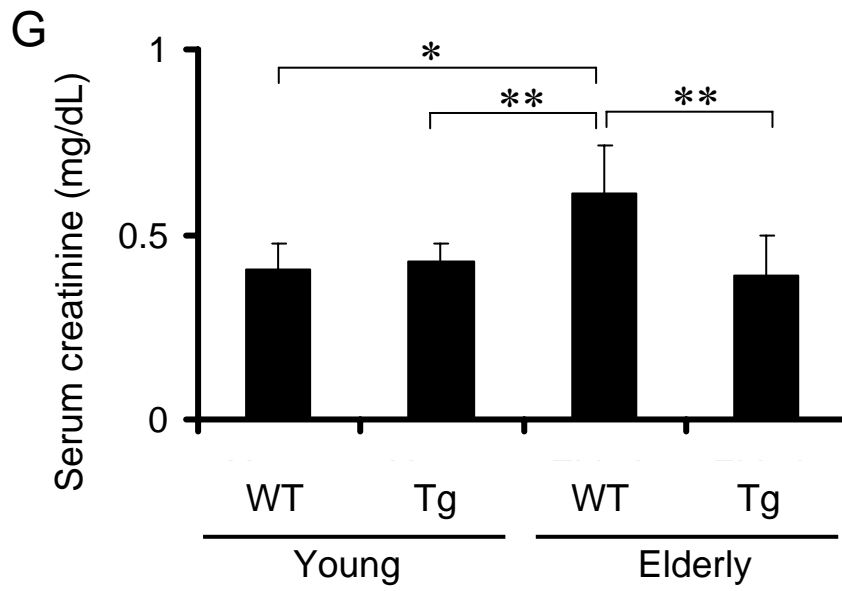
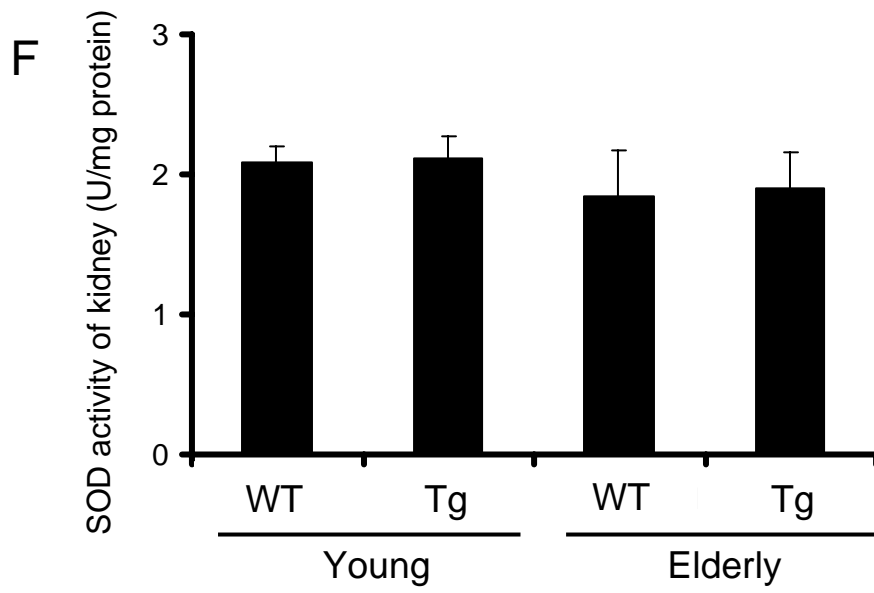
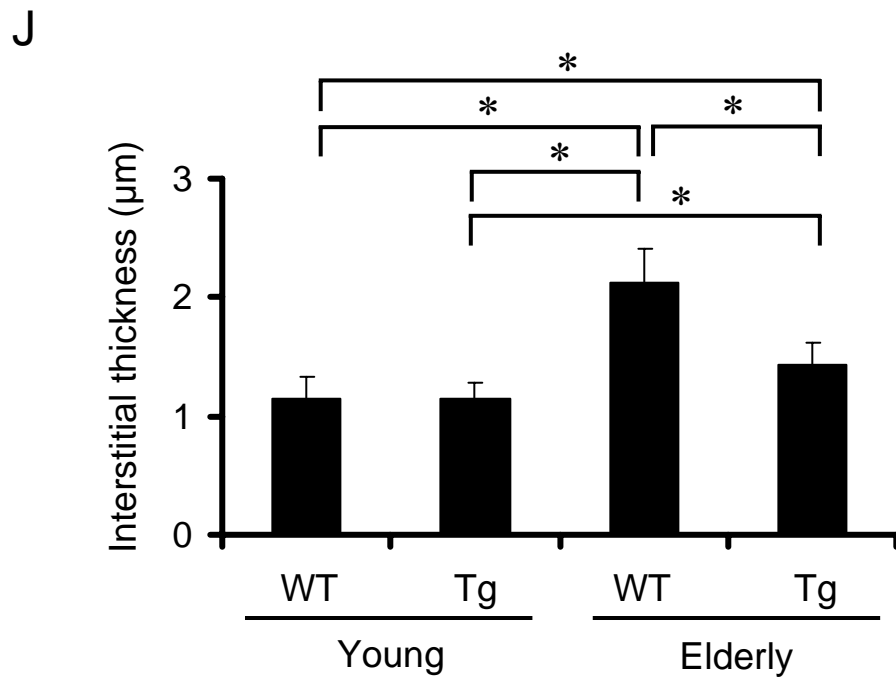
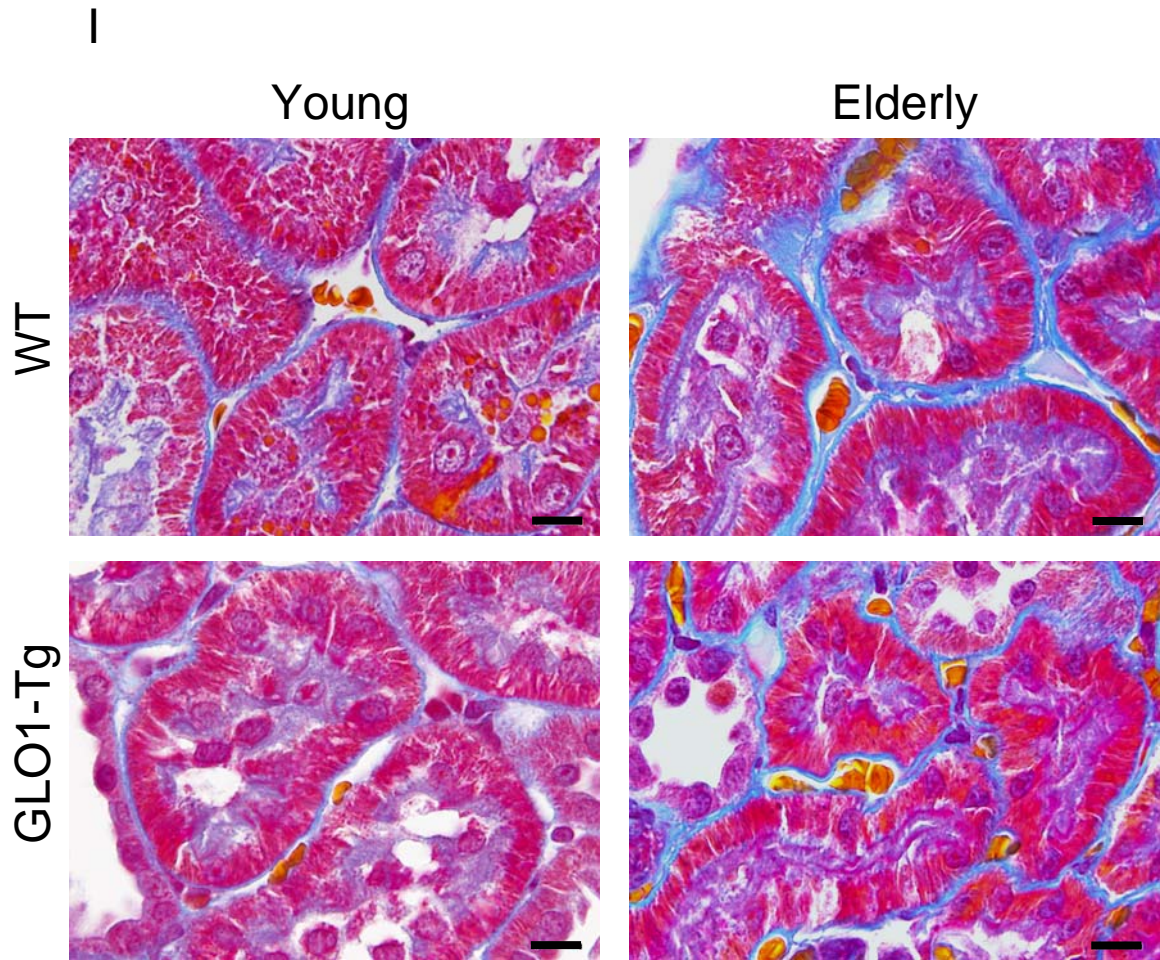


Figure 6

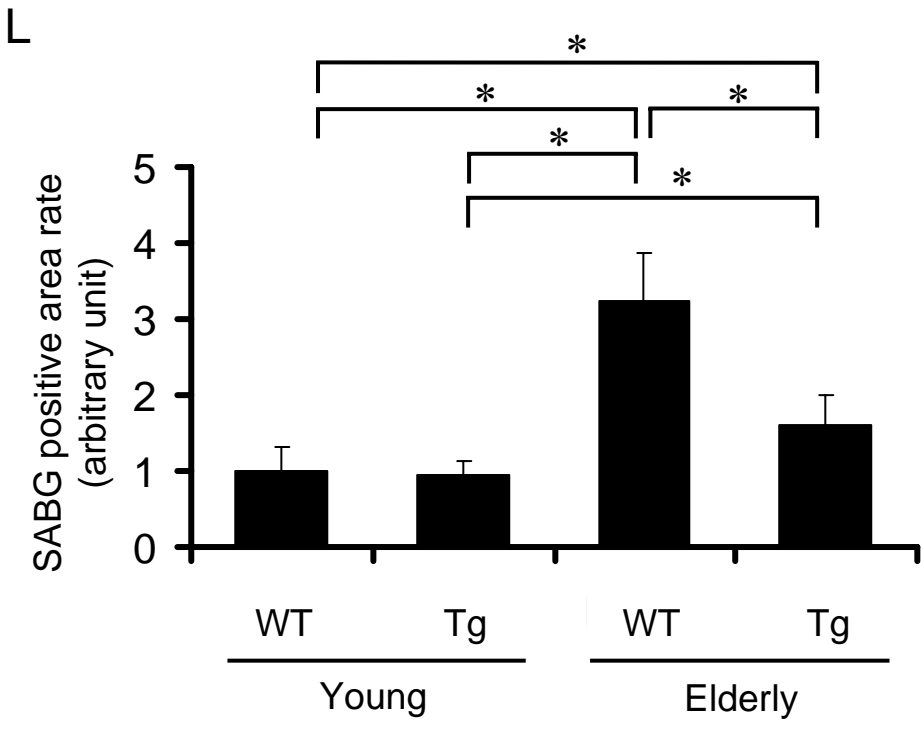
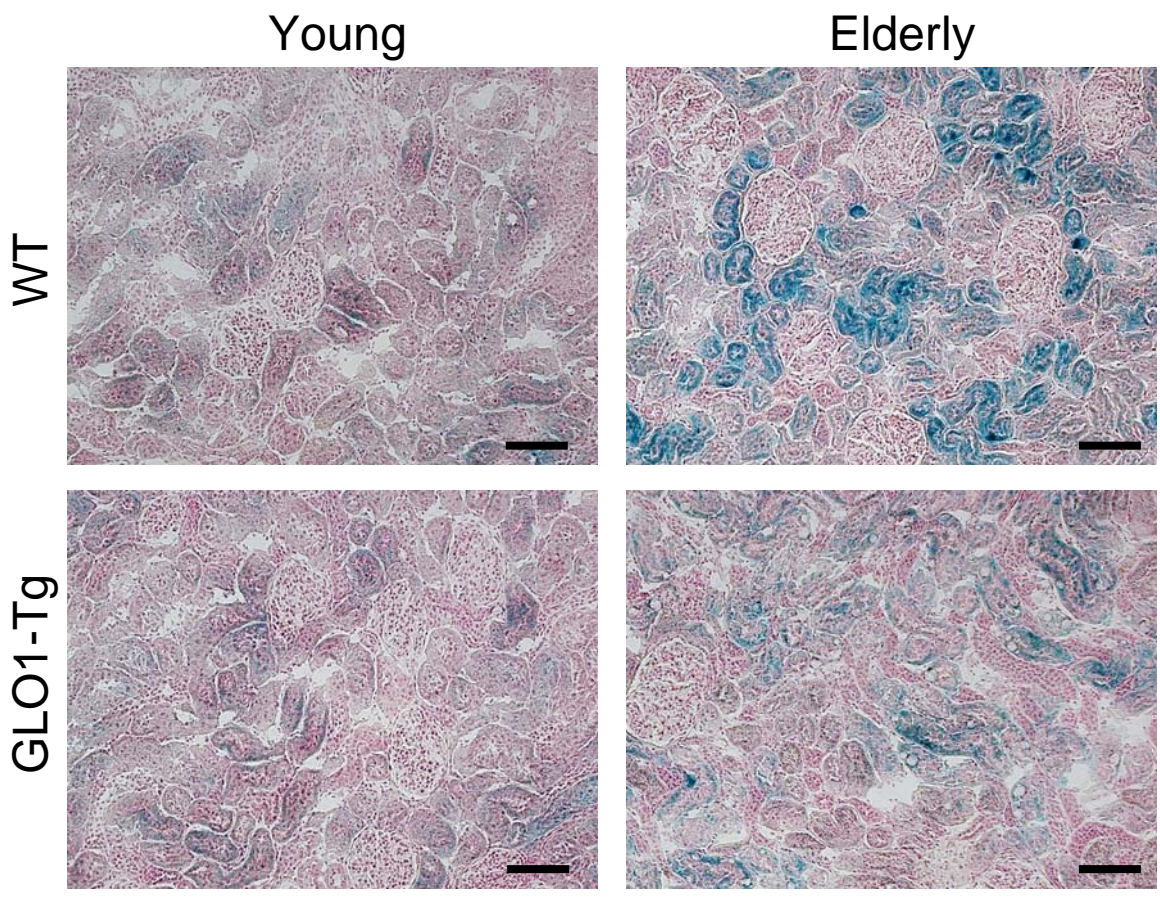




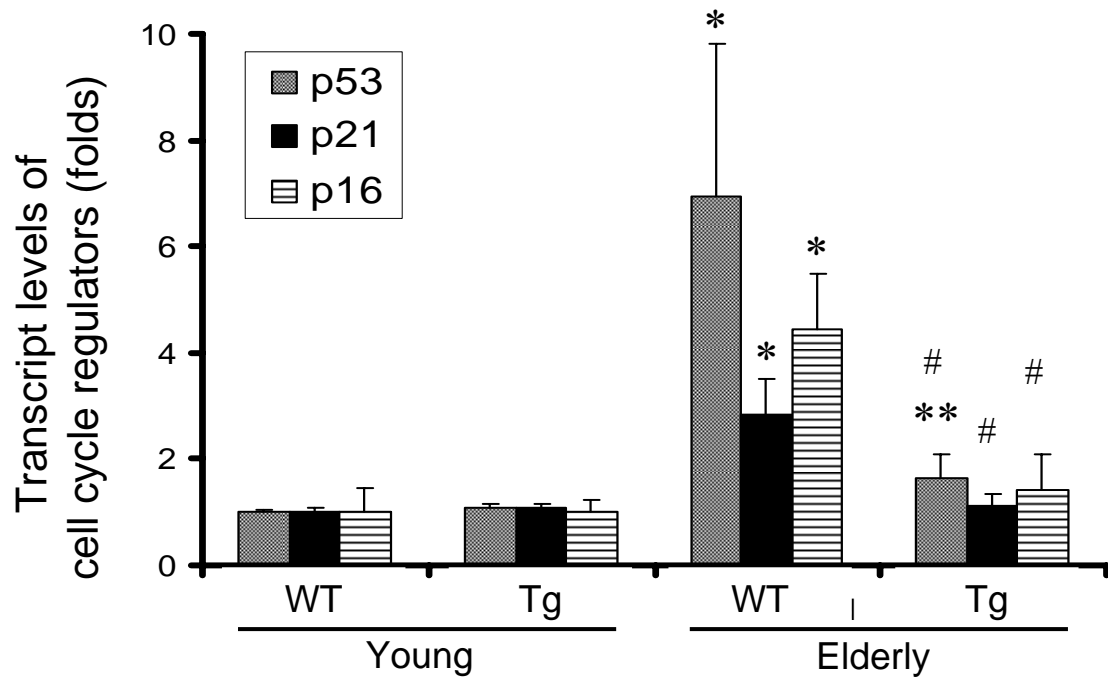




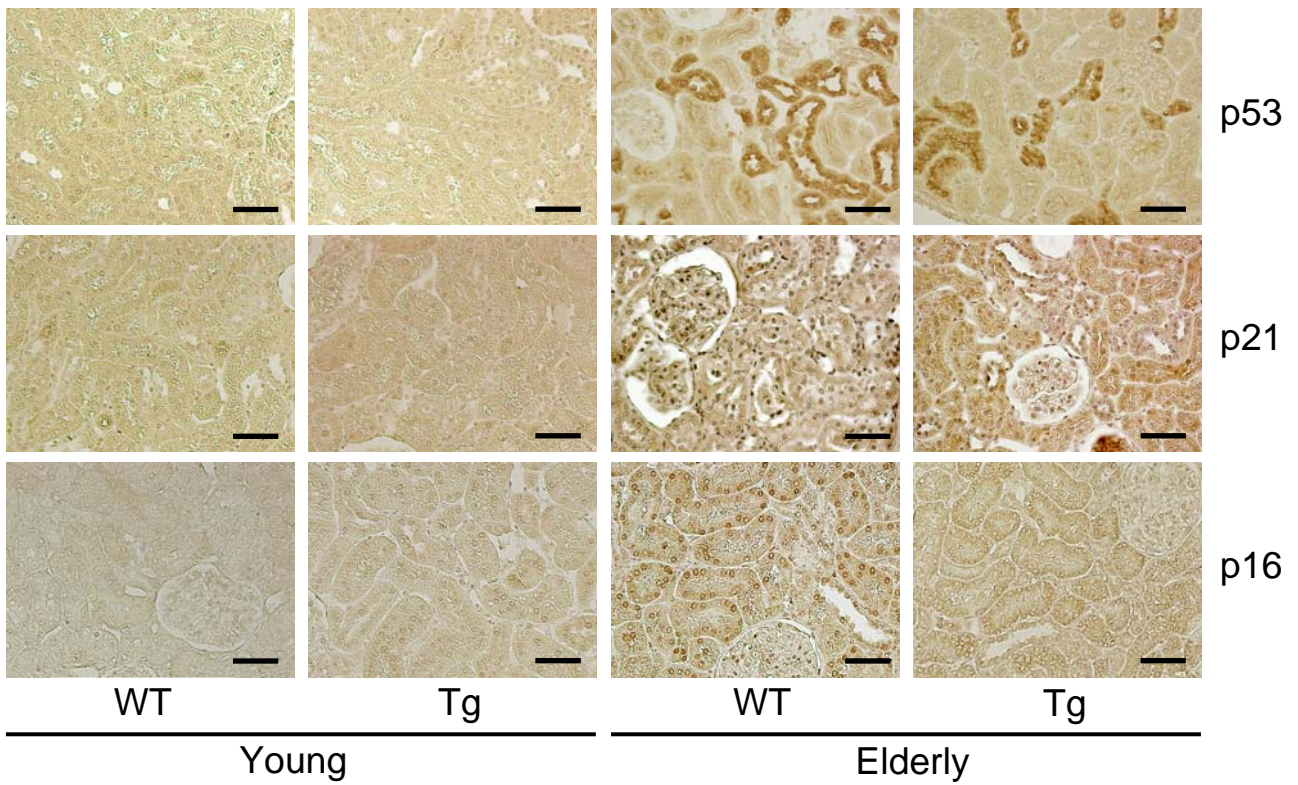
K



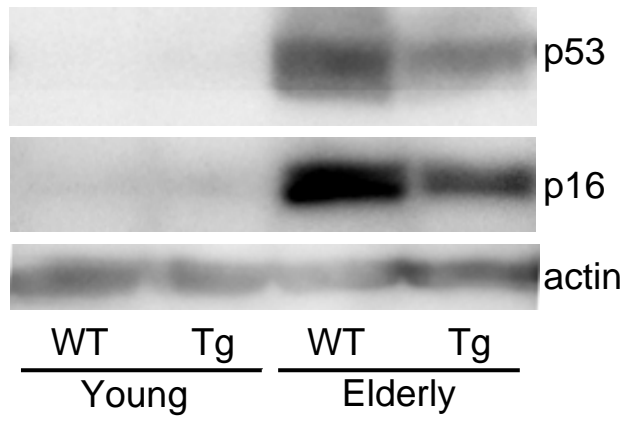
M



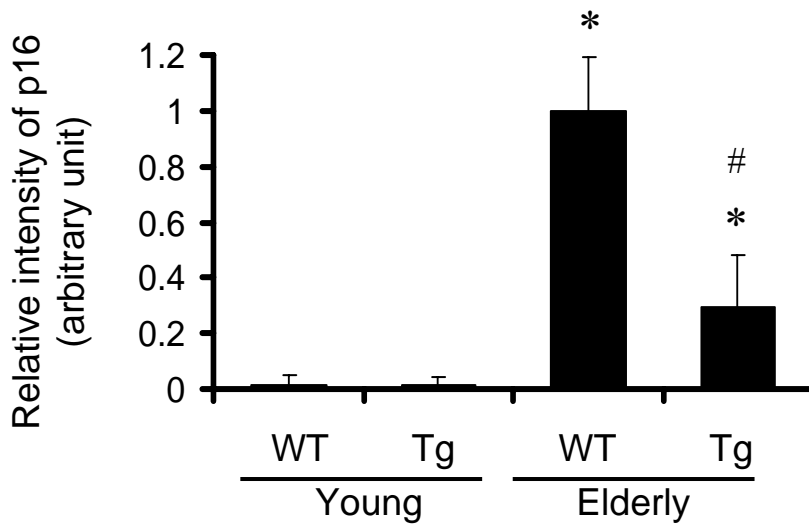
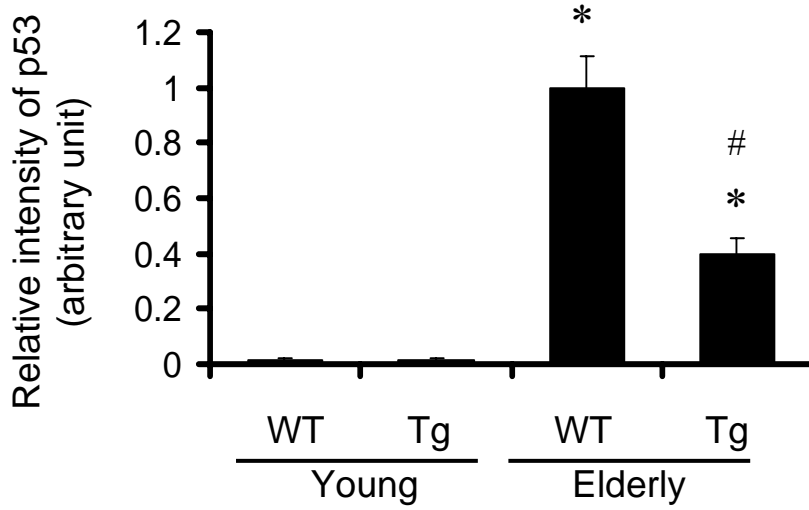
N



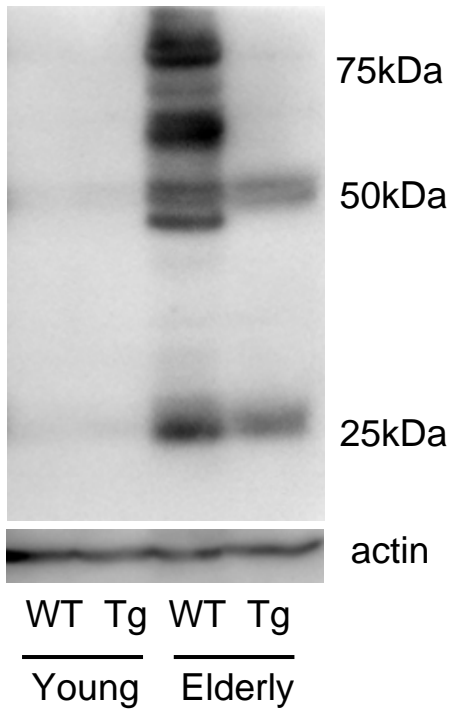
O



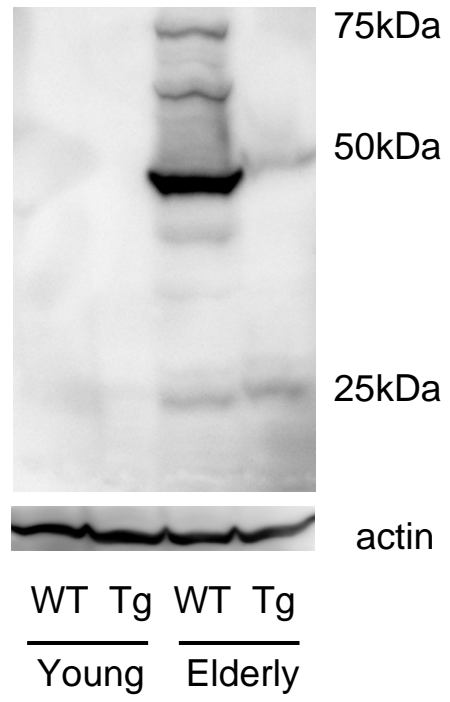
P



Q



S



R

